

# Monocarboxylate transporter 4 deficiency enhances high-intensity interval training-induced metabolic adaptations in skeletal muscle

Yuki Tamura<sup>1,2,3,4,5,6</sup> , Eunbin Jee<sup>2</sup>, Karina Kouzaki<sup>3,7,8</sup>, Takaya Kotani<sup>3</sup> and Koichi Nakazato<sup>2,3,7,8</sup> 

<sup>1</sup>Faculty of Sport Science, Nippon Sport Science University, Tokyo, Japan

<sup>2</sup>Graduate School of Health and Sport Science, Nippon Sport Science University, Tokyo, Japan

<sup>3</sup>Research Institute for Sport Science, Nippon Sport Science University, Tokyo, Japan

<sup>4</sup>Sport Training Center, Nippon Sport Science University, Tokyo, Japan

<sup>5</sup>High Performance Center, Nippon Sport Science University, Tokyo, Japan

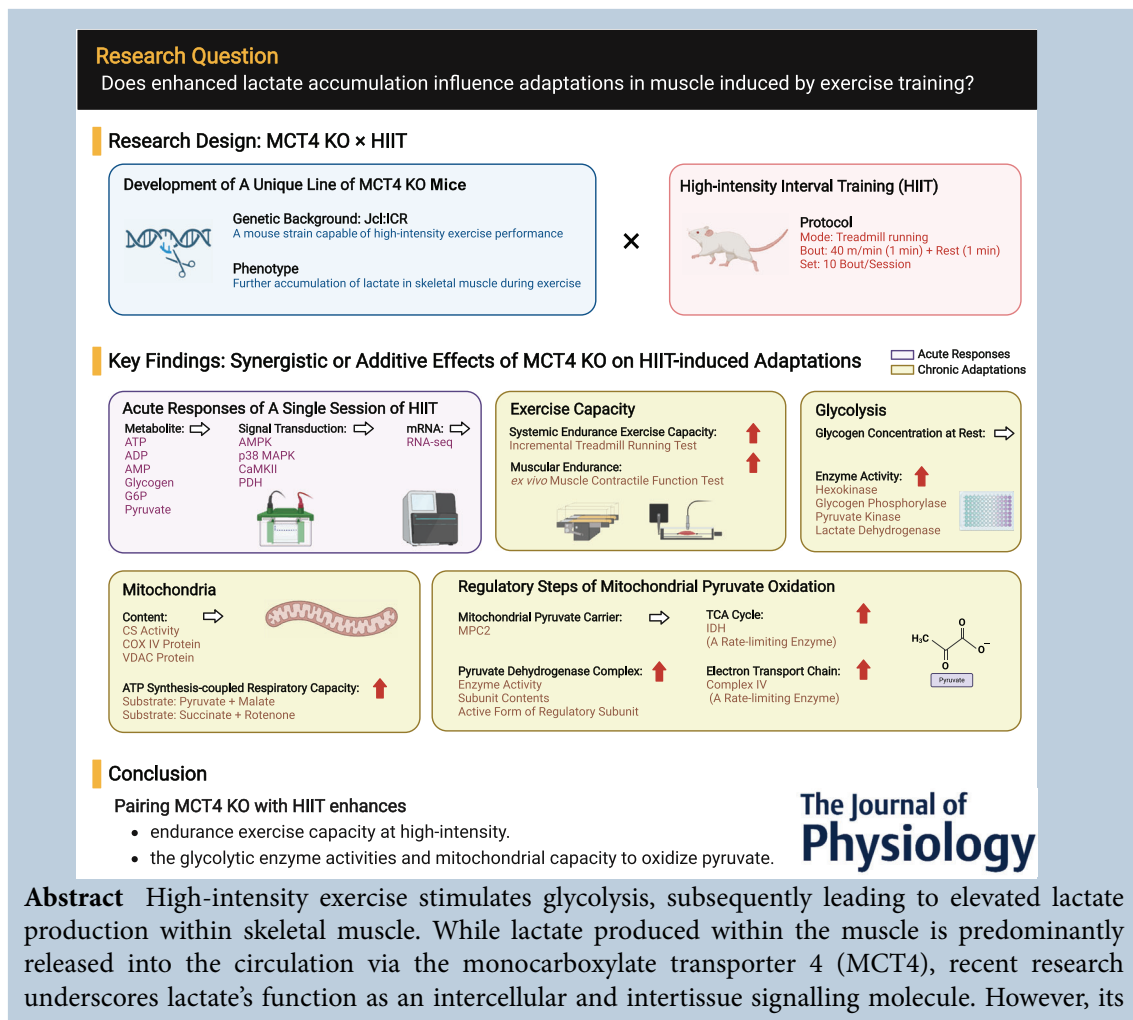
<sup>6</sup>Center for Coaching Excellence, Nippon Sport Science University, Tokyo, Japan

<sup>7</sup>Faculty of Medical Science, Nippon Sport Science University, Tokyo, Japan

<sup>8</sup>Graduate School of Medical and Health Science, Nippon Sport Science University, Tokyo, Japan

Handling Editors: Karyn Hamilton & Mark Viggars

The peer review history is available in the Supporting Information section of this article (<https://doi.org/10.1113/JP285719#support-information-section>).



**Abstract** High-intensity exercise stimulates glycolysis, subsequently leading to elevated lactate production within skeletal muscle. While lactate produced within the muscle is predominantly released into the circulation via the monocarboxylate transporter 4 (MCT4), recent research underscores lactate’s function as an intercellular and intertissue signalling molecule. However, its

specific intracellular roles within muscle cells remains less defined. In this study, our objective was to elucidate the effects of increased intramuscular lactate accumulation on skeletal muscle adaptation to training. To achieve this, we developed MCT4 knockout mice and confirmed that a lack of MCT4 indeed results in pronounced lactate accumulation in skeletal muscle during high-intensity exercise. A key finding was the significant enhancement in endurance exercise capacity at high intensities when MCT4 deficiency was paired with high-intensity interval training (HIIT). Furthermore, metabolic adaptations supportive of this enhanced exercise capacity were evident with the combination of MCT4 deficiency and HIIT. Specifically, we observed a substantial uptick in the activity of glycolytic enzymes, notably hexokinase, glycogen phosphorylase and pyruvate kinase. The mitochondria also exhibited heightened pyruvate oxidation capabilities, as evidenced by an increase in oxygen consumption when pyruvate served as the substrate. This mitochondrial adaptation was further substantiated by elevated pyruvate dehydrogenase activity, increased activity of isocitrate dehydrogenase – the rate-limiting enzyme in the TCA cycle – and enhanced function of cytochrome *c* oxidase, pivotal to the electron transport chain. Our findings provide new insights into the physiological consequences of lactate accumulation in skeletal muscle during high-intensity exercises, deepening our grasp of the molecular intricacies underpinning exercise adaptation.

(Received 6 October 2023; accepted after revision 29 February 2024; first published online 21 March 2024)

**Corresponding author** Y. Tamura: Nippon Sport Science University, 7-1-1, Fukasawa, Setagaya, Tokyo 158-8508, Japan. Email: y-tamura@nittai.ac.jp

**Abstract figure legend** In this investigation, we explored the impact of increased lactate accumulation in skeletal muscle on its adaptation to training. To address this query, we pioneered a unique line of monocarboxylate transporter 4 (MCT4, a transporter responsible for lactate efflux from cells) knockout mice specifically tailored to the ICR strain, an optimal background for high-intensity exercise studies. These MCT4-deficient mice were then subjected to high-intensity interval training (HIIT). Our findings revealed that the synergistic effect of MCT4 deficiency coupled with HIIT notably enhanced the endurance capacity of the mice during high-intensity exercise. This effect is likely due to the augmented activity of glycolytic enzymes and improved mitochondrial capacity for pyruvate oxidation.

### Key points

- We pioneered a unique line of monocarboxylate transporter 4 (MCT4) knockout mice specifically tailored to the ICR strain, an optimal background for high-intensity exercise studies.
- A deficiency in MCT4 exacerbates the accumulation of lactate in skeletal muscle during high-intensity exercise.
- Pairing MCT4 deficiency with high-intensity interval training (HIIT) results in a synergistic boost in high-intensity exercise capacity, observable both at the organismal level (via a treadmill running test) and at the muscle tissue level (through an *ex vivo* muscle contractile function test).
- Coordinating MCT4 deficiency with HIIT enhances both the glycolytic enzyme activities and mitochondrial capacity to oxidize pyruvate.

**Yuki Tamura** completed his BSc at Nippon Sport Science University in 2011 (Prof. Makoto Ohno's lab.) and PhD at the University of Tokyo in 2016 (Prof. Hideo Hatta's lab.). He was a JSPS Postdoctoral Fellow, researching at Nippon Sport Science University (Prof. Koichi Nakazato's lab.) and York University (Prof. David A. Hood's lab.) until 2018. Since then, he has served as an Assistant and now Associate Professor at Nippon Sport Science University. His current research interest lies in exercise metabolism, specifically targeting mitochondria-centered bioenergetics in skeletal muscle.



## Introduction

As exercise intensity increases, glycolysis is more highly activated and the production of lactate in skeletal muscle is increased. Lactate has been considered a product of anaerobic metabolism and a causative agent of muscular fatigue (Cairns, 2006). However, more than a century of scientific contributions have now disproved this concept, and the actual role of lactate is being revealed. Lactate is a temporally and spatially dynamic metabolite which is not only transported within cells but also between cells and between tissues (Brooks, 1986, 2000, 2018). Lactate is transported by monocarboxylate transporters (MCTs) (Garcia et al., 1994). MCTs transport lactate with protons, and the direction of transport is determined by a concentration gradient. To date, 14 MCT isoforms have been identified. Among the MCT isoforms, MCT1 and MCT4 have garnered significant attention due to their distinct molecular properties and adaptabilities in the context of exercise biochemistry and muscle physiology (Dubouchaud et al., 2000; Thomas et al., 2012). MCT1, characterized by a high affinity for lactate ( $K_m$ : 3.5 mM), is predominantly expressed in oxidative muscle (Bonen, 2001; Bröer et al., 1998). Conversely, MCT4, which exhibits a lower affinity for lactate ( $K_m$ : 17–34 mM), is primarily found in glycolytic muscle (Bonen, 2001; Dimmer et al., 2000). These molecular distinctions suggest that MCT1 primarily facilitates the uptake of lactate in skeletal muscle, whereas MCT4 is more involved in lactate efflux.

The lactate shuttle via the circulation plays a crucial role in ensuring the proper systemic energy metabolism by providing substrate for gluconeogenesis and oxidation in mitochondria. In recent years, lactate has also been recognized for its potential role as a signalling molecule. Researchers have studied the effects of increased lactate concentrations in the extracellular fluid or blood on the recipient cells and tissues. For instance, exogenous lactate administration has been shown to increase the content and function of mitochondria in skeletal muscle, promote beige adipogenesis and improve neuronal function (Carrière et al., 2014; Kitaoka et al., 2016; Magistretti & Allaman, 2018; Takahashi et al., 2020; Takahashi et al., 2022). Moreover, lactate functions as an intracellular signalling molecule, potentially modulating biological processes such as mitochondrial oxidative substrate selection,  $\text{NAD}^+$ / $\text{NADH}$  and reactive oxygen species (ROS) production and histone modifications (Brooks, 2020; Hashimoto et al., 2007; Philp et al., 2005; Zhang et al., 2019). These processes may be direct or secondary drivers of subsequent cellular adaptations. However, the scientific understanding of lactate's role as a signalling molecule within skeletal muscle cells still remains unclear. To better comprehend lactate's function within cells, it is crucial to conduct experiments that

inhibit the lactate-releasing transporter MCT4. Recently, Bisetto and colleagues reported that MCT4-deficient mice, with C57BL/6NTac genetic background, exhibit a decrease in running performance on a treadmill (Bisetto et al., 2019). The authors suggested that the underlying physiological basis is morphological and functional insufficiency of the neuromuscular junction, rather than alterations in skeletal muscle size and contractile properties (Bisetto et al., 2019). Nonetheless, the impact of MCT4 deficiency on skeletal muscle is still not fully understood, particularly regarding whether MCT4 deficiency-induced further accumulation of lactate during exercise promotes bioenergetic remodelling or affects exercise training-induced functional adaptations in skeletal muscle.

This study aimed to investigate the impact of MCT4 deficiency-induced further lactate accumulation in skeletal muscle on high-intensity interval training (HIIT)-induced muscle adaptation. To address this, we developed an MCT4-deficient mouse model with a Jcl:ICR genetic background capable of high-intensity exercise performance. We found that MCT4 deficiency enhances HIIT-induced improvement of endurance exercise capacity at high intensity. Furthermore, it was also shown that the combination of MCT4 deficiency and HIIT increases the glycolytic enzyme activity and the mitochondrial oxidative capacity for pyruvate.

## Methods

### Ethical approval

All animal experiments were approved by the Animal Experimental Committee of Nippon Sport Science University (no. 020-A05). The authors have read, and all experiments complied with, the policies and regulations of the *Fundamental Guidelines for Proper Conduct of Animal Experiments and Related Activities in Academic Research Institutions* published by the Ministry of Education, Culture, Sports, Science and Technology, Japan (no. 71, 2006). In addition, this study was conducted in adherence with The Journal of Physiology's guidelines for animal experiments.

### Experimental animals

Eight-week-old male C57BL/6J and Jcl:ICR mice were purchased from CLEA Japan. The mice were housed in a 12-h light–dark cycle (dark: 18.00–06.00 h) at 22°C. They had access to standard chow (CE-2, CLEA Tokyo, Japan) and water *ad libitum*. The treadmill-based exercise experiment was conducted during a specific time window, from 09.00 to 11.00 h. Using the CRISPR/Cas9 system, we developed MCT4-deficient mice with a Jcl:ICR genetic background. All mice were sacrificed by cervical dislocation. Detailed information on the number of mice

used in each experiment was provided within figure legends.

### Development of MCT4 knockout mouse

**crRNA design.** Using the CRISPR/Cas9 system, we developed MCT4-deficient mice with a Jcl:ICR genetic background. Following the KOnezumi algorithm (Kuno et al., 2019), we designed crRNA (Integrated DNA Technology (IDT), Coralville, IA, USA) to remove the region of Exon3-5 of *Slc16a3* (crRNA-left: GAGGGCTGCTTTCACCTGAG, crRNA-right: CAGCACTCACCTCCTGACGG).

**Preparation of gRNA-Cas9 RNP solution.** We mixed 1.5  $\mu$ l of 100  $\mu$ M crRNA and 100  $\mu$ M tracrRNA (IDT) each and incubated them in a thermal cycler at 95°C for 5 min, then left them at room temperature for another 5 min to prepare complete gRNA. To 3  $\mu$ l of the gRNA solution, we added 1  $\mu$ l of Cas9 protein (10 mg/ml, 1081059, IDT) and incubated it at room temperature for 10 min. We then mixed 4  $\mu$ l of each left and right gRNA-Cas9 RNP solution, added 1  $\mu$ l of OptiMEM (31985062, Thermo Fisher Scientific, Waltham, MA, USA) and 1  $\mu$ l of FastGreen FCFsolution (061-00031, Fujifilm Wako Pure Chemical Corp., Tokyo, Japan) to make the final solution.

**i-GOAND method.** We developed MCT4 knockout mice using i-GONAD technology (Ohtsuka et al., 2018). We cohabited male and female Jcl:ICR mice at 17.00 h, and female mice with visible vaginal plugs at 09.00 h the next day were considered as successful mating. Mated female mice were anaesthetized by intraperitoneal injection of 0.75 mg/kg medetomidine hydrochloride, 4 mg/kg midazolam and 5 mg/kg butorphanol tartrate at 15.00 h. We made an incision from the backside, exposed the ovaries and oviduct ampulla and injected 2  $\mu$ l of the CRISPR RNP solution from the ovarian side of the oviduct towards oviduct ampulla using a glass capillary. Immediately afterward, we clamped the oviduct ampulla with tweezers-type electrodes and then introduced the gRNA-Cas9 solution into the embryo with an electroporator (NEPA21, Nepagene, Chiba, Japan) connected to the electrodes. The electroporation parameters were configured as follows: For the poring pulse, the settings were a voltage of 40 V, pulse duration of 5 ms, pulse interval of 50 ms, with a total of 3 repeats, a decay rate of 10%, and alternating polarity (+/-). For the transfer pulse, the parameters were set to a voltage of 10 V, pulse duration of 50 ms, pulse interval of 50 ms, with 6 repeats, a decay rate of 40%, and also alternating polarity (+/-). We returned the ovaries and oviduct back into the body, intraperitoneally injected the anaesthetic antagonist

(0.75 mg/kg atipamezole hydrochloride) and woke the mouse up.

**Genotyping.** We extracted gDNA from the tails of the born mice using a commercial DNA extraction kit. The extracted DNA was amplified by PCR using Tks Gflex DNA Polymerase (R060A, Takara Bio, Shiga, Japan). Primers that span the removal region (Fwd: TTAAACGTAGCCAGGGGTGG, Rev: GGAAGTGCCTCAGACATGCA) were designed (PCReady, Eurofins Genomics, Tokyo, Japan). PCR product lengths were determined using agarose electrophoresis with fluorescent DNA-binding dyes (Midori Green Advance, Nippon Genetics, Tokyo, Japan). Furthermore, by sequencing the PCR product, we identified the specific removal region. Confirmation of knockouts for RNA and protein analysis followed the procedure described below.

**Breeding.** We backcrossed the G0 generation KO mice with at least two generations of wild-type mice to obtain heterozygous mice. By mating these heterozygous mice, we obtained MCT4-deficient mice and wild-type littermates, which were used for experiments.

### Incremental exercise test

**Acclimatization.** Three days before the exercise performance test, the mice were acclimatized to the treadmill every 24 h. In acclimatization, the mice were made to run for 5 min at 5 m/min, 5 min at 10 m/min and 5 min at 15 m/min.

**Main test.** After a 24-h interval from the final acclimatization, we carried out the incremental exercise performance test. The running speed was increased by 4 m/min every 3 min starting from 5 m/min. The blood lactate concentration was measured immediately after the end of each stage using a portable device (Lactate Pro 2, Arkray, Kyoto, Japan) from the tail vein. If the mouse was exhausted, the test was terminated and the maximal speed and running distance were recorded. The maximum speed achieved during the treadmill running test was defined as the highest speed at which they could successfully complete a full 3-min stage. For example, if a mouse manages to run for 3 min at a speed of 40 m/min but fails to sustain 44 m/min for more than 1 min in the subsequent stage, the highest attained speed is recorded as 40 m/min. The point of exhaustion was determined when the mouse remained in continuous contact with the treadmill's rear wall for a duration exceeding 2 s. If carried out after the end of the training intervention, a 24-h interval was given from the end of the final training session.

### High-intensity interval training

A set was defined as running for 1 min at a speed of 40 m/min, followed by 1 min of rest. This was carried out for 10 sets. In the case of a single session of high-intensity interval exercise, the mice were euthanized by cervical dislocation immediately after or 3 h after completing 10 sets, and the skeletal muscles (gastrocnemius) were collected. To evaluate long-term adaptation, training sessions were carried out five times a week for 3 weeks. Twenty-four hours after the end of the final training session, an incremental exercise performance test was carried out or the mice were euthanized by cervical dislocation and the skeletal muscles (gastrocnemius or extensor digitorum longus (EDL)) were collected.

### Ex vivo muscle contractile function

We measured contractile function at isolated muscle following a previously reported paper (Park et al., 2012). Mice were anaesthetized as described above, and the EDL muscle was carefully dissected from tendon to tendon. The tendons on both ends of the EDL were fixed with thread and mounted in a tissue bath chamber for force measurement. The thread tied to the proximal tendon of the EDL was connected to a force transducer. Additionally, platinum electrodes connected to an isolator were positioned to both sides of the EDL. The EDL was allowed to equilibrate in Tyrode solution, saturated with 100% oxygen (2.5 mM  $\text{Ca}^{2+}$  Tyrode solution: 140 mM NaCl, 5 mM KCl, 10 mM HEPES, 2.5 mM  $\text{CaCl}_2$ , 2 mM  $\text{MgCl}_2$  and 10 mM glucose), for 10 min. The length of the EDL that produces the maximum twitch tension when subjected to an electrical pulse at 1 Hz was fine-tuned as the optimal length. The time to onset contraction, time to peak force and half-relaxation time at maximum twitch tension were calculated. The relationship between force and frequency was evaluated by delivering electrical pulses at frequencies ranging from 1 to 250 Hz at 1-min intervals, and the tension during these times was recorded. The maximum tetanic force and the ratio of force at each frequency to the maximum tetanic tension were calculated. The muscle force during twitch and tetanic contractions was normalized to the physiological cross-sectional area of the EDL: cross-sectional area = (muscle mass, in grams)/[1.06 g/cm<sup>3</sup> × (optimal fiber length, in cm)].

### Myofibre cross-sectional area

Cross-sections of the gastrocnemius muscle (10  $\mu\text{m}$  thick) were cut in a cryostat (CM1860, Leica Biosystems, Nussloch, Germany) at  $-26^\circ\text{C}$ , fixed in 4% paraformaldehyde phosphate buffer solution (161-20141, Fujifilm Wako Pure Chemical Corp.) and washed in

0.1 M phosphate buffer (PB; pH 7.4). These sections were blocked with a blocking reagent (Toyobo, Tokyo, Japan) for 1 h at room temperature and then incubated with primary rabbit IgG polyclonal anti-laminin antibody (L9393, Sigma-Aldrich, St Louis, MO, USA; dilution 1:2000), and diluted in Can Get Signal reagent 1 (Toyobo) overnight at  $4^\circ\text{C}$ . After incubation, the sections were washed in 0.1 M PB, incubated for 1 h in the dark at room temperature with a secondary antibody (A-21441, Alexa Fluor 488 chicken anti-rabbit IgG; Thermo Fisher Scientific, Waltham, MA, USA; dilution 1:500) diluted in Can Get Signal reagent 2 (Toyobo), and washed again in 0.1 M PB. The sections were mounted on slides with coverslips using PermaFluor Aqueous Mounting Medium (TA-030-FM, Thermo Fisher Scientific). Slides were imaged using a confocal laser scanning microscope (FV3000; Olympus, Tokyo, Japan). Analysis of fibre cross-sectional areas was performed using MyoVision software (Ver. 1.0, Windows) (Wen et al., 2018).

### Protein extraction and western blot

Protein extraction and western blotting analysis were performed as described previously (Uno et al., 2022). Briefly, gastrocnemius muscle was homogenized in radio-immunoprecipitation assay buffer (188-02453, Fujifilm Wako Pure Chemical Corp.) containing a protease and phosphate inhibitor cocktail (169-26063/167-24381, Fujifilm Wako Pure Chemical Corp.). The protein concentration was measured using the bicinchoninic acid (BCA) method (295-78401, Fujifilm Wako Pure Chemical Corp.). Equal amounts (2.5–10  $\mu\text{g}$ ) of protein were separated using standard SDS-PAGE on 10% (w/v) Stain-free TGX polyacrylamide gels (161-0173, Bio-Rad Laboratories, Hercules, CA, USA) and transferred to polyvinylidene difluoride membranes (IPVH00010, Sigma-Aldrich). Protein transfer was confirmed by staining with Ponceau S (33427.01, SERVA Electrophoresis GmbH, Heidelberg, Germany). The membranes were blocked with blocking reagent (NYPBR01, Toyobo) for 1 h and incubated for 1 h with primary antibodies diluted in Can Get signal reagent 1 (NKB-101, Toyobo). The antibodies used in this study are listed in Table 1. After incubation, the membranes were washed with Tris-buffered saline containing 0.01% Tween 20 (TBST, T9142, Takara Bio), then incubated for 1 h at room temperature with the secondary antibodies (7074/7076, Cell signalling Technology, Danvers, MA, USA) diluted in Can Get signal reagent 2 (NKB-101, Toyobo) and washed again with TBST. Chemiluminescent reagents (Super-Signal West Pico Chemiluminescent Substrate; Thermo Fisher Scientific) were used for protein detection. The blots were scanned and quantified using ChemiDoc XRS (170-8071, Bio-Rad) and Image Lab (12012931, version

**Table 1. Antibodies used in this study**

Antibody	Supplier	ID
Rabbit-polyclonal anti-phospho-pyruvate dehydrogenase alpha 1 (Ser293)	Cell Signaling Technology	Cat. no.: 31866, RRID:AB_2799014
Rabbit-monoclonal anti-pyruvate dehydrogenase alpha 1	Cell Signaling Technology	Cat. no.: 3205, RRID:AB_2162926
Rabbit-monoclonal anti-phospho-acetyl-CoA carboxylase (Ser79)	Cell Signaling Technology	Cat. no.: 11818, RRID:AB_2687505
Rabbit-monoclonal anti-acetyl-CoA carboxylase	Cell Signaling Technology	Cat. no.: 3676, RRID:AB_2219397
Rabbit-monoclonal anti-phospho-p38 MAPK (Thr180/Tyr182)	Cell Signaling Technology	Cat. no.: 4511, RRID:AB_2139682
Rabbit-monoclonal anti-p38 MAPK	Cell Signaling Technology	Cat. no.: 8690, RRID:AB_10999090
Rabbit-monoclonal anti-phospho-CaMKII (Thr286)	Cell Signaling Technology	Cat. no.: 12716, RRID:AB_2713889
Rabbit-monoclonal anti-CaMKII	Cell Signaling Technology	Cat. no.: 4436, RRID:AB_10545451
Rabbit-polyclonal anti-GLUT4	Proteintech	Cat. no.: 66846-1-Ig, RRID:AB_2882186
Rabbit-polyclonal anti-MCT1	Proteintech	Cat. no.: 20139-1-AP, RRID:AB_2878645
Rabbit-polyclonal anti-MCT4	Proteintech	Cat. no.: 22787-1-AP, RRID:AB_11182479
Rabbit-polyclonal anti-CD36	Proteintech	Cat. no.: 18836-1-AP, RRID:AB_10597244
Rabbit-monoclonal anti-COX IV	Cell Signaling Technology	Cat. no.: 4850, RRID:AB_2085424
Rabbit-monoclonal anti-VDAC	Cell Signaling Technology	Cat. no.: 12454, RRID:AB_2797922
Rabbit-monoclonal anti-MPC1	Cell Signaling Technology	Cat. no.: 14462, RRID:AB_2773729
Rabbit-monoclonal anti-MPC2	Cell Signaling Technology	Cat. no.: 46141, RRID:AB_2799295
Rabbit-polyclonal anti-DLAT	Proteintech	Cat. no.: 13426-1-AP, RRID:AB_2091774
Rabbit-polyclonal anti-DLD	Proteintech	Cat. no.: 16431-1-AP, RRID:AB_2091888
Rabbit-polyclonal anti-PDK2	Proteintech	Cat. no.: 15647-1-AP, RRID:AB_2268006
Rabbit-polyclonal anti-PDK4	Proteintech	Cat. no.: 12949-1-AP, RRID:AB_2161499
Rabbit-polyclonal anti-PDP1	Proteintech	Cat. no.: 21176-1-AP, RRID:AB_2878824
Mouse-monoclonal anti-Total OXPHOS Rodent WB Antibody Cocktail	Abcam	Cat. no.: ab110413, RRID:AB_2629281
Rabbit-polyclonal anti-laminin	Sigma-Aldrich	Cat. no.: L9393, RRID:AB_477163
Chicken anti-rabbit IgG (H + L) cross-adsorbed secondary antibody, Alexa Fluor™ 488	Thermo Fisher Scientific	Cat. no.: A-21441, RRID:AB_2535859
Anti-rabbit IgG, HRP-linked antibody	Cell Signaling Technology	Cat. no.: 7074, RRID:AB_2099233
Anti-mouse IgG, HRP-linked antibody	Cell Signaling Technology	Cat. no.: 7076, RRID:AB_330924

CaMKII, Ca<sup>2+</sup>-calmodulin-dependent protein kinase II; COX IV, cytochrome c oxidase subunit IV; DLAT, dihydrolipoamide S-acetyltransferase; DLD, dihydrolipoamide dehydrogenase; GLUT4, glucose transporter 4; HRP, horseradish peroxidase; MAPK, mitogen-activated protein kinase; MPC, mitochondrial pyruvate carrier; PDK, pyruvate dehydrogenase kinase; PDP1, pyruvate dehydrogenase phosphatase 1; VDAC, voltage-dependent anion channel. Abcam, Cambridge, MA, USA; Cell Signaling Technology, Danvers, MA, USA; Proteintech, Rosemont, IL, USA; Sigma-Aldrich, St Louis, MO, USA; Thermo Fisher Scientific, Waltham, MA, USA.

6.1, Windows; Bio-Rad), and we used the stain-free signal (25–150 kDa) intensity as a loading control.

### RNA extraction and gene expression assays

**RNA extraction.** RNA samples were prepared as described previously (Kasai et al., 2022; Kotani et al., 2019). Gastrocnemius muscle was homogenized in TRIzol reagent (Thermo Fisher Scientific) on ice and separated into organic and aqueous phases using chloroform. RNA was isolated from the aqueous phase following precipitation with ethanol with a commercial kit (FG-80050, Nippon Genetics, Tokyo, Japan). The RNA concentration and purity were measured by spectrophotometry (Nanodrop One, Thermo Fisher Scientific).

**cDNA synthesis and real-time qPCR.** cDNA synthesis from 1 µg of total RNA was performed with random hexamer primers using a commercial kit (FSQ-201, Toyobo). The gene expression of interest was quantified using qPCR reagent (QPS-101, Toyobo) and a thermal cycler with optical reaction module (CFX96 Touch, Bio-Rad). All samples were run in duplicate simultaneously with a negative control that contained no cDNA. Transcripts of TATA binding protein (*Tbp*) was used as a control housekeeping gene, the expression of which did not change among groups. The sequences of primers we used in this study are as follows: *Slc16a3*-Fwd: TATCCAGATCTACCTCACAC, *Slc16a3*-Rev: GGCCTGGCAAAGATGTCGATGA, *Tbp*-Fwd: CTGCCACACCAGCTTCTGA, *Tbp*-Rev: TGCAGCAAATCGCTTGGG. Primer specificities were confirmed by dissociation curve at each PCR run. Quantification was by the calibration curve method.

**RNA-seq and bioinformatics.** RNA-seq libraries were prepared as described previously (Tamura et al., 2020). Briefly, sequencing libraries for gene expression profiling (3' mRNA-seq) were prepared using a commercial kit (QuantSeq 3'mRNA-seq Library Prep Kit FWD for Illumina, Lexogen, Inc., Vienna, Austria). First-strand DNA was synthesized from 2 µg RNA template with oligodT primers containing the Illumina-specific Read2 linker sequence. After removal of the RNA template, the second strand was synthesized using random primers containing the Illumina-specific Read1 linker sequence. Double-stranded cDNA libraries were washed and purified with magnetic beads. After purification, the libraries were amplified by PCR with primers containing an adaptor and the i7 index sequence. Libraries were purified with magnetic beads, quantified using a fluorometer (Qubit 4, Thermo Fisher Scientific), and pooled by adjusting to an equimolar concentration. Sequencing

was performed using a MiniSeq High Output Reagent Kit (75 cycles) on a MiniSeq system (Illumina, CA, USA). After sequencing, the sequencing quality was examined using FastQC. Adaptor sequences and the poly A sequence were trimmed using cutadapt, mapped to the reference sequence using Salmon, and the read number was counted. Data of raw read counts from each sample were normalized by the rlog algorithm (gene median; minimal counts per million: 0.5). Further bioinformatics were conducted by integrated differential expression and pathway analysis (Ge et al., 2018). Differential gene expression analyses were conducted using DESeq2 (false discovery rate cutoff: 0.1; minimal fold change: 1.5).

### Metabolite assay

**Glucose and lactate concentrations in blood.** The concentrations of glucose and lactate in the blood were measured using a portable measuring device (Glutest Neo Alpha, Sanwa Kagaku Kenkyusho, Aichi, Japan), utilizing blood samples drawn from the tail vein of the mice.

**Glycogen concentration assay.** A glycogen concentration assay was performed as described previously with minor modifications (Tamura et al., 2020). Gastrocnemius muscle was homogenized in KOH saturated with NaSO<sub>4</sub> and incubated at 95°C. Ethanol was added to the resuspension, the resuspension was centrifuged and the supernatant was discarded. Pellets were incubated at 37°C for 1 h to evaporate the supernatant. Pellets were resuspended in HCl and incubated at 95°C for 2 h to convert glycogen into glucose. The glucose concentration in the suspension was measured using a commercial kit (298-65701, Fujifilm Wako Pure Chemical Corp.).

**Sample preparation for intramuscular metabolite assays.** Gastrocnemius muscle was homogenized in 0.6 M HClO<sub>4</sub> buffer. Centrifugation was performed at 12,000 g for 15 min at 4°C, and the supernatant was collected. The supernatant was neutralized using 1 M NaOH. Samples were analysed to measure AMP, ADP, ATP, glucose-6-phosphate, pyruvate and lactate.

**ATP, ADP and AMP concentrations.** ATP, ADP and AMP concentration assays of cells were performed as described previously with minor modifications (Hoxhaj et al., 2017). AMP and ADP in the samples were converted to ATP by using a reaction buffer (1 unit/50 µl of myokinase (M3003, Sigma-Aldrich), 0.25 unit of pyruvate kinase (P9136, Sigma-Aldrich), 0.2 mM dCTP (77104, Thermo Fisher Scientific), 0.3 mM phosphoenolpyruvate (P7127, Sigma-Aldrich). ADP in the samples was also converted to ATP using a reaction buffer (0.25 unit of pyruvate kinase (305-50711, Fujifilm Wako Pure Chemical Corp.), 0.2 mM

dCTP, 0.3 mM phosphoenolpyruvate (160-14763, Fujifilm Wako Pure Chemical Corp.). The ATP concentration in each sample was then measured with a commercially available luminescence-based kit (G9241, Promega, Madison, WI, USA). The concentrations of AMP and ADP were calculated from the difference in ATP concentration between the enzymatically processed samples.

**Glucose-6-phosphate concentration.** A glucose-6-phosphate concentration assay of cells was performed as described previously with minor modifications (Matsunaga et al., 2021). Briefly, 10  $\mu$ l of standard glucose-6-phosphate solution or sample was incubated with 90  $\mu$ l of reaction buffer (50 mM Tris-HCl, 20  $\mu$ M MgCl<sub>2</sub>, 25  $\mu$ M NADP<sup>+</sup>, 0.5 mM WST-3 (345-08881, Fujifilm Wako Pure Chemical Corp.), 10  $\mu$ M 1-methoxy-5-methylphenazinium methylsulfate (345-04001, Fujifilm Wako Pure Chemical Corp.) and 1 U/ $\mu$ l glucose-6-phosphate dehydrogenase, pH 8.0). Absorbance at 433 nm was measured after incubation for 30 min at room temperature in the dark.

**Pyruvate concentration.** A pyruvate concentration assay of cells was performed as described previously with minor modifications (Zhu et al., 2010). Briefly, 10  $\mu$ l of standard sodium pyruvate solution or sample was incubated with 90  $\mu$ l of reaction buffer (100 mM potassium phosphate with 1.0 mM EDTA, pH 6.7, 1.0 mM MgCl<sub>2</sub>, 10  $\mu$ M FAD, 0.2 mM thiamine pyrophosphate, 200 U/ $\mu$ l pyruvate oxidase (PYO-311, Toyobo), 50  $\mu$ M Amplex Red (A12222, Thermo Fisher Scientific), 1 U/ml Horseradish peroxidase (169-10791, Fujifilm Wako Pure Chemical Corp.). After incubation for 30 min at room temperature in the dark, fluorescence at 590 nm was measured at excitation of 535 nm using a microplate reader (Spark, Tecan, Männedorf, Switzerland).

**Lactate concentration.** A lactate concentration assay of culture medium and cell lysates was performed as described previously (Tamura et al., 2020). Briefly, 10  $\mu$ l of the standard sodium lactate solution or cell culture medium was incubated with 90  $\mu$ l of the reaction buffer (2 U/ml LDH, 0.4 M hydrazine and 2.5 mM NAD<sup>+</sup>, pH 9.0). After completion of the NAD<sup>+</sup> reduction reaction, which was confirmed by kinetic analysis, the final absorbance at 340 nm was measured using the microplate reader.

**NAD<sup>+</sup> and NADH concentration.** The NAD<sup>+</sup> and NADH were measured using a commercial kit according to the manufacturer's instructions (347-09321, Fujifilm Wako Pure Chemical Corp.).

## Mitochondrial respiratory function

**Mitochondrial isolation.** Mitochondria were isolated by differential centrifugation as previously (Wakabayashi et al., 2020). Briefly, freshly excised gastrocnemius muscle was immediately placed in ice-cold buffer (PBS, 10 mM EDTA, pH 7.4), minced with scissors, supplemented with 0.025% trypsin, and then incubated on ice for 5 min. After tissue suspensions were centrifuged at 200 g for 5 min at 4°C, the supernatants were discarded. Tissue precipitate was homogenized using a Tenbroeck tissue grinder (Wheaton, NJ, USA) with 10 strokes in a buffer (50 mM MOPS, 100 mM KCl, 1 mM EGTA, 5 mM MgSO<sub>4</sub> and 2.0 g/l BSA, pH 7.1). The homogenates were centrifuged at 500 g for 15 min at 4°C twice to collect supernatants containing mitochondria. The supernatants were re-centrifuged at 10,000 g for 15 min at 4°C to obtain the mitochondrial pellets. The mitochondrial pellets were washed with buffer (50 mM MOPS, 100 mM KCl, 1 mM EGTA and 5 mM MgSO<sub>4</sub>) and resuspended in buffer (60 mM potassium lactobionate, 110 mM sucrose, 20 mM HEPES, 10 mM KH<sub>2</sub>PO<sub>4</sub>, 3 mM MgCl<sub>2</sub>, 0.5 mM EGTA and 1 g/l BSA, pH 7.4). The protein concentration was determined using the BCA protein assay. For the respiratory function assays, the protein concentration of the mitochondrial solution was adjusted to 1.0 mg/ml.

**Mitochondrial oxygen consumption rate.** Mitochondrial respiration was measured as described previously (Tamura et al., 2020). Mitochondrial oxygen consumption rate (OCR) was measured using a multimode plate reader (Spark 20M, Tecan) with oxygen monitoring on a 96-well microplate (OP96C, PreScan Precision Sensing GmbH, Regensburg, Germany) (Ex: 540 nm/Em: 650 nm). The substrates used to measure the mitochondrial OCR were 10 mM pyruvate (29805-22, Nacalai Tesque, Kyoto, Japan) + 5 mM malate (138-07512, Fujifilm Wako Pure Chemical Corp.), 10 mM glutamate (072-00501, Fujifilm Wako Pure Chemical Corp.) + 5 mM malate, 200  $\mu$ M octanoylcarnitine (50892, Sigma-Aldrich) + 5 mM malate and 10 mM succinate (199-03305, Fujifilm Wako Pure Chemical Corp.) + 0.5  $\mu$ M rotenone (599-10811, Fujifilm Wako Pure Chemical Corp.). To induce ATP production-coupled respiration (state 3), 2.5 mM ADP (01652-24, Nacalai Tesque) was added. Mineral oil was added to the upper layer of the reaction mixture to prevent contact between the reaction mixture and the air. The relative change in fluorescence per min was measured and converted to the oxygen consumption rate in accordance with the manufacturer's instructions.

**Mitochondrial ROS emission rate.** Mitochondrial ROS emission rate was measured as previously described with minor modifications (Nogami et al., 2021). Briefly, mitochondria (10  $\mu$ g) were incubated in a black 96-well

plate with mitochondrial respiration buffer containing each substrate described above, 5  $\mu$ M Amplex Red, 1 U/ml horseradish peroxidase and 5 U/ml superoxide dismutase (192-11281, Fujifilm Wako Pure Chemical Corp.). The kinetics of ROS emission were assessed under state 3 respiratory conditions through the addition of 2.5 mM ADP. The relative changes in fluorescence per minute were measured using a fluorescence plate reader (Spark 20M, Tecan) (excitation (Ex): 560 (20) nm; emission (Em): 620 (20) nm). The relative change in fluorescence per minute was measured and normalized to OCR.

### Enzymatic activity (phosphagen system and glycolysis)

**Sample preparation.** Supernatants obtained by the 500 g centrifugation step of the mitochondrial fractionation procedure (post-nuclear fraction) were used for the measurement of enzyme activities. Their protein concentrations were determined using the BCA method and adjusted to 1.0 mg/ml.

**Creatine kinase.** A creatine kinase activity assay was performed as described previously with minor modifications (Takahashi et al., 2022a). Ten micrograms of protein was mixed with reaction buffer (50 mM Tris-HCl, 2.5 mM ADP, 10 mM MgCl<sub>2</sub>, 30 mM phosphocreatine (032-04583, Fujifilm Wako Pure Chemical Corp.), 30 mM glucose (132-001751, Fujifilm Wako Pure Chemical Corp.), 1 mM NADP<sup>+</sup> (308-50463, Fujifilm Wako Pure Chemical Corp.), 20 mM N-acetyl-L-Cysteine (NAC) (015-05132, Fujifilm Wako Pure Chemical Corp.), 2 mM EDTA (345-01865, Fujifilm Wako Pure Chemical Corp.), 1 mM AMP (303-50491, Fujifilm Wako Pure Chemical Corp.), 1 U/ $\mu$ l glucose-6-phosphate dehydrogenase (074-04101, Fujifilm Wako Pure Chemical Corp.) and 3 U/ $\mu$ l hexokinase (302-51681, Fujifilm Wako Pure Chemical Corp.), pH 8.0) in a 96-well plate. Absorbance changes at 340 nm per min were calculated.

**Adenylate kinase.** An adenylate kinase activity assay was performed as described previously with minor modifications (Takahashi et al., 2022a). Ten micrograms of protein was mixed with reaction buffer (50 mM Tris-HCl, 2.5 mM ADP, 10 mM MgCl<sub>2</sub>, 30 mM glucose, 1 mM NADP<sup>+</sup>, 1 U/ $\mu$ l glucose-6-phosphate dehydrogenase and 3 U/ $\mu$ l hexokinase, pH 8.0) in a 96-well plate. Absorbance changes at 340 nm per min were calculated.

**Hexokinase.** A hexokinase activity assay was performed as described previously with minor modifications (Takahashi et al., 2022b). Ten micrograms of protein

was mixed with reaction buffer (50 mM Tris-HCl, 1 mM ATP, 10 mM MgCl<sub>2</sub>, 30 mM glucose, 1 mM NADP<sup>+</sup> and 1 U/ $\mu$ l glucose-6-phosphate dehydrogenase, pH 8.0) in a 96-well plate. Absorbance changes at 340 nm per min were calculated.

**Glycogen phosphorylase.** A glycogen phosphorylase activity assay was performed as described previously (Wilson, 2021). Ten micrograms of protein was mixed with reaction buffer (20 mM PIPES (348-08251, Fujifilm Wako Pure Chemical Corp.), 0.8% glycogen (074-05561, Fujifilm Wako Pure Chemical Corp.), 50 mM sodium phosphate, 200  $\mu$ M NADP<sup>+</sup>, 500  $\mu$ M glucose-1,6-bisphosphate (G6893, Sigma-Aldrich), 1 U/ $\mu$ l glucose-6-phosphate dehydrogenase and 3 U/ $\mu$ l phosphoglucomutase (P3397, Sigma-Aldrich), pH 8.0) in a 96-well plate; 3 mM AMP was added to stimulate enzymatic activity. Absorbance changes at 340 nm per min were calculated.

**Phosphofructokinase.** A phosphofructokinase activity assay was performed as described previously with minor modifications (Takahashi et al., 2022b). Ten micrograms of protein was mixed with reaction buffer (10 mM Tris-HCl, 1 mM ATP, 7 mM phosphoenolpyruvate (160-14763, Fujifilm Wako Pure Chemical Corp.), 200  $\mu$ M NADH (305-50451, Fujifilm Wako Pure Chemical Corp.), 10 mM fructose-6-phosphate (066-05341, Fujifilm Wako Pure Chemical Corp.), 5  $\mu$ M KCl, 2 mM MgSO<sub>4</sub>, 1 U/ $\mu$ l pyruvate kinase (305-50711, Fujifilm Wako Pure Chemical Corp.) and 1 U/ $\mu$ l lactate dehydrogenase (300-52721, Fujifilm Wako Pure Chemical Corp.), pH 8.0) in a 96-well plate. Absorbance changes at 340 nm per min were calculated.

**Pyruvate kinase.** A pyruvate kinase activity assay was performed as described previously with minor modifications (Wubben et al., 2020). Ten micrograms of protein was mixed with reaction buffer (50 mM HEPES, 100 mM MgCl<sub>2</sub>, 5  $\mu$ M KCl, 7 mM phosphoenolpyruvate, 200  $\mu$ M NADH, 2.5 mM ADP and 1 U/ $\mu$ l lactate dehydrogenase, pH 8.0) in a 96-well plate. Absorbance changes at 340 nm per min were calculated.

**Citrate synthase (post-nuclear fraction).** A citrate synthase activity assay was performed as described previously (Matsunaga et al., 2022). Ten micrograms of protein was mixed with reaction buffer (50 mM Tris-HCl, 100  $\mu$ M 5,5'-Dithiobis(2-nitrobenzoic acid) (DTNB) (346-08551, Dojindo Molecular Technologies, Inc., Kumamoto, Japan), 300  $\mu$ M acetyl-CoA (00546-54, Nacalai Tesque), 50  $\mu$ M oxaloacetate (25804-81, Nacalai Tesque) and 0.01% Triton X-100, pH 7.4) in a 96-well

plate. Absorbance changes at 412 nm per min were calculated.

**Lactate dehydrogenase (lactate to pyruvate).** A lactate dehydrogenase (lactate to pyruvate) activity assay was performed as described previously (Tamura et al., 2020). Ten micrograms of protein was mixed with reaction buffer (10 mM sodium lactate, 0.4 M hydrazine and 2.5 mM NAD<sup>+</sup>, pH 9.0) in a 96-well plate. Absorbance changes at 340 nm per min were calculated.

**Lactate dehydrogenase (pyruvate to lactate).** A lactate dehydrogenase (pyruvate to lactate) activity assay was performed as described previously (Tamura et al., 2020). Ten micrograms of protein was mixed with reaction buffer (50 mM Tris-HCl, 10 mM sodium pyruvate (195-05965, Fujifilm Wako Pure Chemical Corp.) and 200 μM NADH, pH 8.0) in a 96-well plate. Absorbance changes at 340 nm per min were calculated.

### Enzymatic activity (mitochondria)

**Sample preparation.** Assays were performed using the mitochondrial fractions obtained during the analysis of mitochondrial respiratory function.

**Pyruvate dehydrogenase.** To measure pyruvate dehydrogenase activity, 10 μg of protein was mixed with reaction buffer (100 mM Tris-HCl, 200 μM thiamine pyrophosphate (T10183, Tokyo Chemical Industry, Tokyo, Japan), 2.5 mM NAD<sup>+</sup>, 100 μM CoA-SH (302-50483, Fujifilm Wako Pure Chemical Corp.), 10 mM sodium pyruvate, 10 mM MgCl<sub>2</sub>, 0.01% Triton X-100, 50 μM 1-methoxy-5-methylphenazinium methylsulfate (341-04003, Fujifilm Wako Pure Chemical Corp.) and 100 μM WST-3 (345-08881, Fujifilm Wako Pure Chemical Corp.), pH 8.0) in a 96-well plate. Absorbance changes at 433 nm per min were calculated.

**Citrate synthase.** A citrate synthase activity assay was performed as described previously (Matsunaga et al., 2022). One microgram of protein was mixed with reaction buffer (50 mM Tris-HCl, 100 μM DTNB (346-08551, Dojindo Molecular Technologies, Inc.), 300 μM acetyl-CoA (00546-54, Nacalai Tesque), 50 μM oxaloacetate (25804-81, Nacalai Tesque) and 0.01% Triton X-100, pH 7.4) in a 96-well plate. Absorbance changes at 412 nm per min were calculated.

**Isocitrate dehydrogenase.** An isocitrate dehydrogenase activity assay was performed as described previously with minor modifications (Muro-pastor & Florencio, 1992). Five micrograms of protein was mixed with reaction buffer (100 mM Tris-HCl, 5 mM isocitrate (19608-51, Nacalai

Tesque), 1 mM NAD<sup>+</sup> and 10 mM MgCl<sub>2</sub> pH 8.0) in a 96-well plate. Absorbance changes at 340 nm per min were calculated.

**α-Ketoglutarate dehydrogenase.** An α-ketoglutarate dehydrogenase activity assay was performed as described previously with minor modifications (Shi et al., 2007). Ten micrograms of protein was mixed with reaction buffer (100 mM Tris-HCl, 200 μM thiamine pyrophosphate, 2.5 mM NAD<sup>+</sup>, 100 μM CoA-SH, 10 mM α-ketoglutarate (19817-82, Nacalai Tesque), 10 mM MgCl<sub>2</sub>, 0.01% Triton X-100, 50 μM 1-methoxy-5-methylphenazinium methylsulfate and 100 μM WST-3, pH 8.0) in a 96-well plate. Absorbance changes at 433 nm per min were calculated.

**Succinate dehydrogenase.** A succinate dehydrogenase (complex II) activity assay was performed as described previously (Wakabayashi et al., 2020). Five micrograms of protein was mixed with reaction buffer (20 mM succinate, 0.015% (w/v) 2,6-dichlorophenolindophenol (591-03541, Fujifilm Wako Pure Chemical Corp.), 12.5 μM decylubiquinone (195-041, 599-10811, Fujifilm Wako Pure Chemical Corp.), 300 μM KCN and 1 mg/ml BSA) in a 96-well plate. Absorbance changes at 600 nm per min were calculated.

**Malate dehydrogenase.** To measure malate dehydrogenase, 10 μg of protein was mixed with reaction buffer (100 mM Tris-HCl, 5 mM malate, 1 mM NAD<sup>+</sup> and 10 mM MgCl<sub>2</sub> pH 8.0) in a 96-well plate. Absorbance changes at 340 nm per min were calculated.

**Complex I.** A complex I activity assay was performed as described previously (Wakabayashi et al., 2020). Ten micrograms of the protein suspension was mixed with reaction buffer (100 μM NADH, 60 μM ubiquinone (C7956, Sigma-Aldrich), 300 μM KCN, 3 mg/ml BSA) in a 96-well plate. Absorbance changes at 340 nm were calculated every minute. Rotenone-sensitive enzyme activity (i.e. rotenone absence – rotenone presence) was regarded as complex I activity.

**Complex I + III.** A complex I + III activity assay was performed as described previously (Wakabayashi et al., 2020). Ten micrograms of protein was mixed with reaction buffer (200 μM NADH, 50 μM cytochrome *c* (C2506, Sigma-Aldrich), 300 μM KCN and 1 mg/ml BSA) in a 96-well plate. Absorbance changes at 550 nm per min were calculated.

**Complex II + III.** A complex II + III activity assay was performed as described previously (Wakabayashi et al., 2020). Ten micrograms of protein was mixed with reaction

buffer (10 mM succinate, 50  $\mu$ M cytochrome *c* and 300  $\mu$ M KCN) in a 96-well plate. Absorbance changes at 550 nm per min were calculated.

**Complex IV.** A complex IV activity assay was performed as described previously with minor modifications (Memme et al., 2022). Ten micrograms of protein was mixed with reaction buffer (50  $\mu$ M cytochrome *c* reduced with dithiothreitol) in a 96-well plate. Absorbance changes at 550 nm per min were calculated.

### Mitochondrial supercomplex assembly

Mitochondrial supercomplex assembly was evaluated as described previously (Wakabayashi et al., 2020). Two-dimensional-PAGE (blue native (BN)-PAGE followed by SDS-PAGE) was conducted to evaluate mitochondrial supercomplex assembly. Isolated mitochondrial fractions (50  $\mu$ g) were mixed with 5% digitonin (digitonin/protein ratio: 8 g/g; BN2006, Thermo Fisher Scientific) and 4 $\times$  sample buffer (BN20032, Thermo Fisher Scientific), and incubated for 30 min on ice. After incubation, the suspensions were centrifuged at 20,000 *g* for 15 min at 4°C. Supernatants were collected and 5% Coomassie G-250 sample additive was applied (BN2004, Thermo Fisher Scientific). Proteins were loaded on 4%–20% gradient gels (4561096, Bio-Rad), and BN-PAGE was performed using buffers for native PAGE (BN2001, Thermo Fisher Scientific). BN-PAGE was followed by SDS-PAGE, and then proteins were transfer to a polyvinylidene difluoride membrane. Standard western blot analysis was performed as described above using an anti-OXPHOS antibody (primary: ab110413 (1:1000), Abcam, Cambridge, MA, USA; secondary: 7076, Cell Signaling Technology).

### Lactate dehydrogenase isozyme

Lactate dehydrogenase isozyme was evaluated as described previously (Tamura et al., 2020). Post-nuclear fraction mixed with glycerol (final concentration: 10%) and bromophenol blue (final concentration: 0.05 mg/ml) was used as sample. Equal amounts of protein (30  $\mu$ g) were separated by native PAGE (7.5% (w/v) TGX polyacrylamide gels) at 12 mV for 100 min. After electrophoresis, gels were incubated in reaction buffer (1 M sodium lactate, 10 mM NAD<sup>+</sup>, 2 mg/ml phenazine-methosulphate and 20 mg/ml tetrazolium-blue) at 37°C until band development.

### Statistical analysis

Data are presented as means  $\pm$  standard deviation. Comparisons between two groups were made using

Student's unpaired *t* test. Analysis of two or three factors was conducted using two-way or three-way analysis of variance (ANOVA), respectively. When an interaction was observed, *post hoc* comparisons were made using the Tukey–Kramer multiple comparisons test. If no interaction was observed, the main effects of each factor were examined. All statistical analyses and graph creation were performed using GraphPad Prism (Ver. 8.4.3, Mac; GraphPad Software Inc., San Diego, CA, USA). Statistical significance was defined as  $P < 0.05$ . *P*-values are provided in each figure.

## Results

### Jcl:ICR strain outperforms C57BL/6J strain in high-intensity exercise and lactate metabolism studies

The C57BL/6J strain is a widely used mouse strain in life sciences due to its genetic background, which is commonly employed for generating genetically modified mice. When studying lactate metabolism during exercise, it is essential for experimental animals to perform high-intensity exercise. However, our experience indicates that the C57BL/6J strain faces difficulties in performing high-intensity exercise. In contrast, we have observed that mice of the Jcl:ICR strain are more adept at high-intensity exercise. We initially investigated whether the Jcl:ICR strain is indeed better suited for high-intensity exercise and lactate metabolism studies than the C57BL/6J strain. Mice of the Jcl:ICR strain tend to have higher body weight and skeletal muscle mass compared to those of the C57BL/6J strain (Fig. 1A–E). Blood lactate concentrations were measured during incremental treadmill running. The results showed that the Jcl:ICR strain achieved higher maximal speed and running distance (calculated as the product of speed and time) than the C57BL/6J strain (Fig. 1F–H). The maximal blood lactate concentration was approximately 10 mmol/L in the C57BL/6J strain, while it reached around 19 mmol/L in the Jcl:ICR strain (Fig. 1I). However, no difference in running speed was observed at the lactate threshold between the two strains (Fig. 1J). These findings suggest that the Jcl:ICR strain has a greater capacity for high-intensity exercise and is more suitable for lactate metabolism studies than the C57BL/6J strain.

### Development of MCT4 knockout mice with Jcl:ICR genetic background using CRISPR/Cas9

We proceeded to generate global MCT4 knockout mice with a Jcl:ICR genetic background using CRISPR/Cas9. Two gRNAs were designed to remove the exon 3 to exon 5 region on the genomic locus of *Slc16a3* gene which encodes the MCT4 protein. (Fig. 2A). This genome

editing led to the removal of 80% of the protein-coding sequence, and frameshift mutations further disrupted the remaining 100% of the protein-coding sequence. We confirmed the successful knockout of MCT4, based on PCR and sequencing analysis of genomic DNA, examination of *Slc16a3* mRNA expression and MCT4 protein expression in gastrocnemius muscle (Fig. 2B–D). Both MCT4 wild-type and MCT4-deficient mice underwent an incremental running test to assess exercise capacity and blood lactate level responses. Maximal speed and running distance were unaffected by MCT4 deficiency, indicating similar exercise capacities between the genotypes (Fig. 2E–G). However, maximal blood lactate concentrations were lower in MCT4-deficient mice (Fig. 2H). These physiological findings further support the successful development of MCT4-deficient mice.

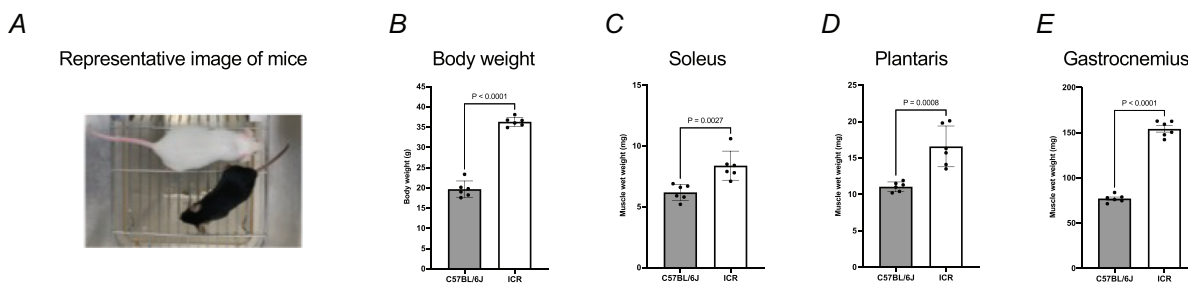
### MCT4 deficiency has minor impact on early physiological response to high-intensity interval exercise

We next investigated whether MCT4 deficiency affects physiological responses to a single bout of high-intensity

interval exercise. MCT4 deficiency further elevated lactate concentration in the gastrocnemius muscle immediately post-exercise (Fig. 3K), while attenuating the increase in blood lactate concentration (Fig. 3C). These findings suggest that high-intensity interval exercise in MCT4-deficient mice serves as a valid model for attenuation of lactate release from skeletal muscle or enhancement of lactate accumulation in skeletal muscle. In contrast, other metabolites in skeletal muscle (ATP, ADP, AMP, Glycogen, glucose-6-phosphate and pyruvate, Fig. 3E–J) and blood glucose (Fig. 3B) showed typical exercise-induced responses, whereas no single effect of MCT4 deficiency and no interaction between MCT4 deficiency and exercise were observed. No effects of exercise or MCT4 deficiency were found on blood free fatty acid concentrations (Fig. 3D) and NAD<sup>+</sup>, NADH and NAD<sup>+</sup>/NADH in gastrocnemius muscle (Fig. 3L–N).

High-intensity interval exercise resulted in decreased phosphorylation status (i.e. inactive status) of pyruvate dehydrogenase-E1 $\alpha$  (PDHE1 $\alpha$ ) levels, which positively regulate carbohydrate oxidation (Rardin et al., 2009) and increased acetyl-CoA carboxylase phosphorylation, indicating activation of AMP-activated protein kinase, an integrative regulatory kinase of energy production

#### Body weight and muscle weight



#### Incremental running test

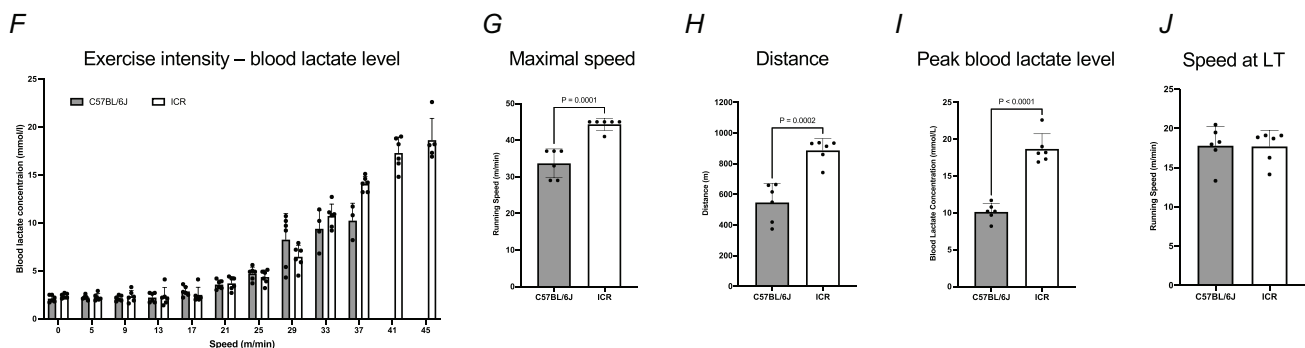


**Figure 1. Mice of the ICR strain are better suited for lactate metabolism studies during exercise than mice of the C57BL/6J strain**

A, representative images of C57BL/6J mouse (bottom: black) and Jcl:ICR mouse (top: white). B–E, comparison of body weight (B), wet muscle weight of soleus (C), plantaris (D) and gastrocnemius (E) between C57BL/6J and Jcl:ICR strains. G–J, relationship between exercise intensity and blood lactate concentration (F), maximal speed (G), distance (H), peak blood lactate concentration (I) and speed at lactate threshold (J) during incremental running test. Data are expressed as means  $\pm$  SD (C57BL/6J:  $n = 6$ , Jcl:ICR:  $n = 6$ ). [Colour figure can be viewed at [wileyonlinelibrary.com](http://wileyonlinelibrary.com)]

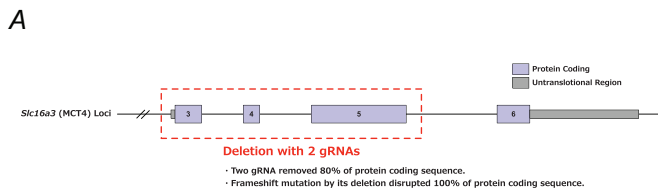
and catabolism during exercise (Marcinko & Steinberg, 2014). These typical metabolic regulatory responses during high-intensity exercise were unaffected by MCT4 deficiency (Fig. 4A–C). Additionally, phosphorylation status (i.e. active status) of exercise-responsive kinases (p38 (mitogen-activated protein kinase and Ca<sup>2+</sup>-calmodulin-dependent protein kinase II) leading to subsequent metabolic adaptations were increased by high-intensity interval exercise (Egan et al., 2010), with no impact from MCT4 deficiency (Fig. 4A, D and E).

We subsequently conducted gene expression profiling 3 h post-exercise to elucidate the changes in gene expression by the singular effect of MCT4 deficiency and the influence of MCT4 deficiency on gene expression changes induced by a single session of high-intensity interval exercise. Principal component analysis revealed a correlation between PC1 and the effects of exercise, while PC2 was significantly associated with the impacts of MCT4 deficiency (Fig. 4F). Only one gene showed increased expression by the interaction between MCT4

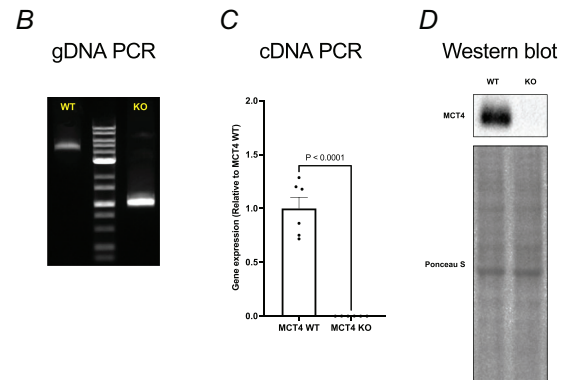
deficiency and high-intensity interval exercise, whereas two genes demonstrated reduced expression (Fig. 4G). On the other hand, the number of genes with changed expression level by the single main effects of MCT4 deficiency and high-intensity interval exercise were 10 and 71, respectively (Fig. 4G). These comprehensive results indicate that (1) the changes in gene expression by the singular effect of MCT4 deficiency are not substantially greater than those by exercise and (2) the impact of MCT4 deficiency on gene expression changes induced by a single bout of high-intensity interval exercise is not interactive and is minor. Full-data on RNA-seq are provided as Supplemental information.

In summary, we examined metabolites, signalling kinase responses and altered gene expression as early responses to high-intensity interval exercise. Deletion of MCT4 resulted in successfully increased lactate level in skeletal muscle associated with exercise, but had no major effect on the initial or early physiological responses to high-intensity interval exercise.

### gRNA design for developing MCT4 knockout mouse



### Validation of successful MCT4 knockout



### Incremental running test

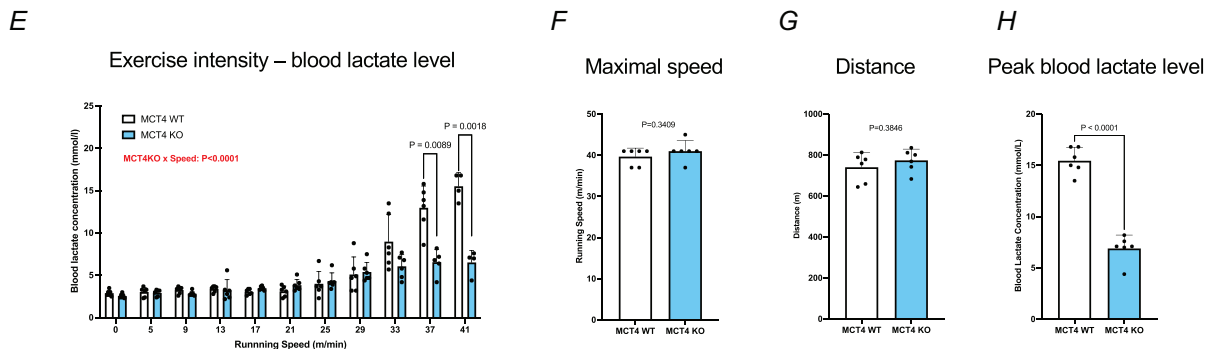


### Figure 2. Development of MCT4 knockout mouse with genetic background of Jcl:ICR

A, gRNA design for developing MCT4 knockout mouse. B–D, validation of successful MCT4 knockout with gDNA PCR (B), cDNA PCR (C) and western blot (D). E–H, relationship between exercise intensity and blood lactate concentration (E), maximal speed (F), distance (G) and peak blood lactate concentration (H) during incremental running test. Data are expressed as means  $\pm$  SD (MCT4 WT:  $n = 6$ , MCT4 KO:  $n = 6$ ). [Colour figure can be viewed at [wileyonlinelibrary.com](http://wileyonlinelibrary.com)]

## MCT4 deficiency and high-intensity interval training synergistically improve endurance exercise capacity at high intensity

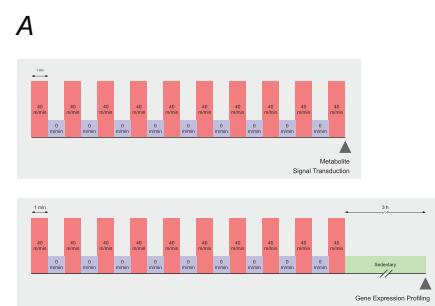
We subsequently investigated whether MCT4 deficiency influences muscle adaptations induced by 3 weeks of HIIT. We observed no effect of training or MCT4 deficiency on body weight and total energy intake (Fig. 5B and C). We then examined skeletal muscle mass and size. No effects of HIIT or MCT4 deficiency on soleus, plantaris or gastrocnemius muscle weights were observed (Fig. 5D–F). These findings are in line with the lack of significant effects of training and MCT4 deficiency on myofibre cross-sectional area in the gastrocnemius muscle (Fig. 5G–I). Overall, the results suggest that 3 weeks of HIIT and/or MCT4

deficiency has no significant impact on skeletal muscle mass and size.

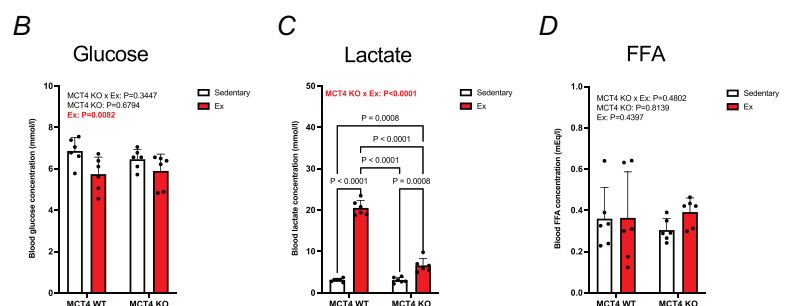
We performed an incremental running MCT4 test before and after the training intervention to evaluate whole-body exercise capacity in mice. The maximally reached speed was increased by HIIT, but was unaffected by MCT4 deficiency (Fig. 6A). However, MCT4 deficiency and training synergistically increased running distance (Fig. 6B). As the results were obtained in the incremental exercise test, they indicate an improvement in endurance exercise capacity at high intensity.

We also examined the contractile properties of isolated skeletal muscle (EDL), excluding potential effects from other organs and/or circulation. Neither training nor MCT4 deficiency affected specific twitch or tetanic

### Experimental procedure



### Metabolite in blood



### Metabolite in muscle

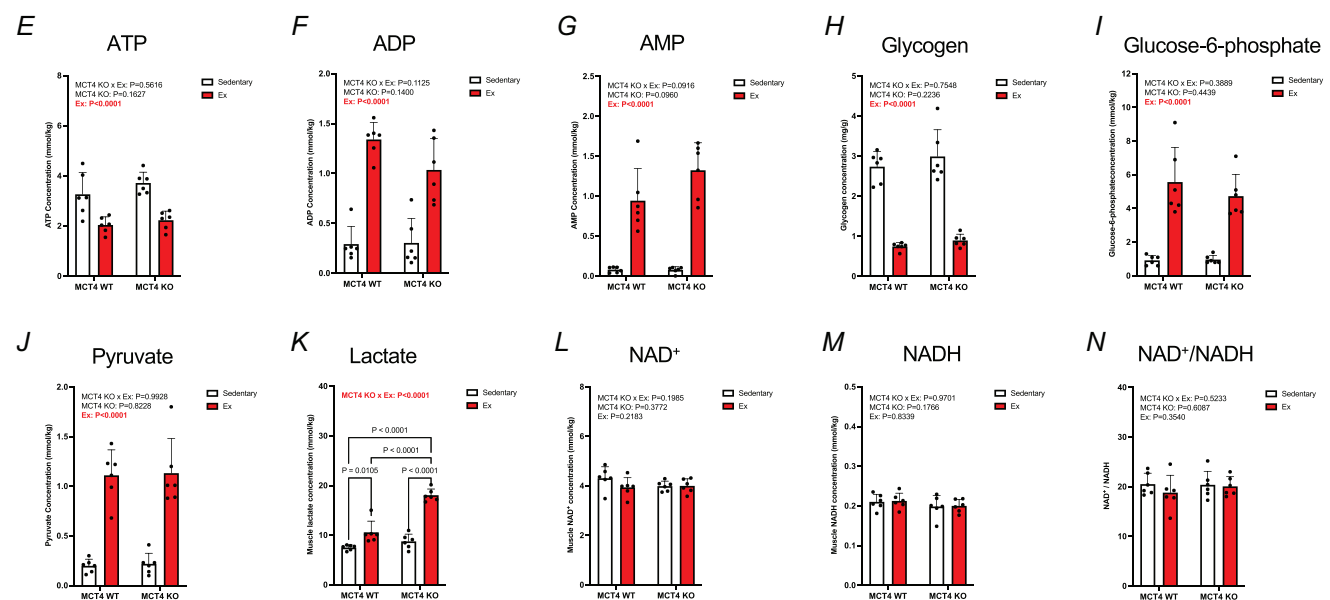


**Figure 3. MCT4 deficiency has little effect on metabolite changes caused by a single bout of high-intensity interval exercise, except for lactate**

A, experimental procedures for a single session of high-intensity interval exercise. B–D, glucose (B), lactate (C) and free fatty acids (D) in blood or plasma immediately after exercise. E–N, ATP (E), ADP (F), AMP (G), glycogen (H), glucose-6-phosphate (I), pyruvate (J), lactate (K), NAD<sup>+</sup> (L), NADH (M) and NAD<sup>+</sup>/NADH (N) in gastrocnemius muscle immediately after exercise. Data are expressed as means ± SD (MCT4 WT/Sedentary: *n* = 6, MCT4 WT/Ex: *n* = 6, MCT4 KO/Sedentary: *n* = 6, MCT4 KO/Ex: *n* = 6). [Colour figure can be viewed at [wileyonlinelibrary.com](http://wileyonlinelibrary.com)]

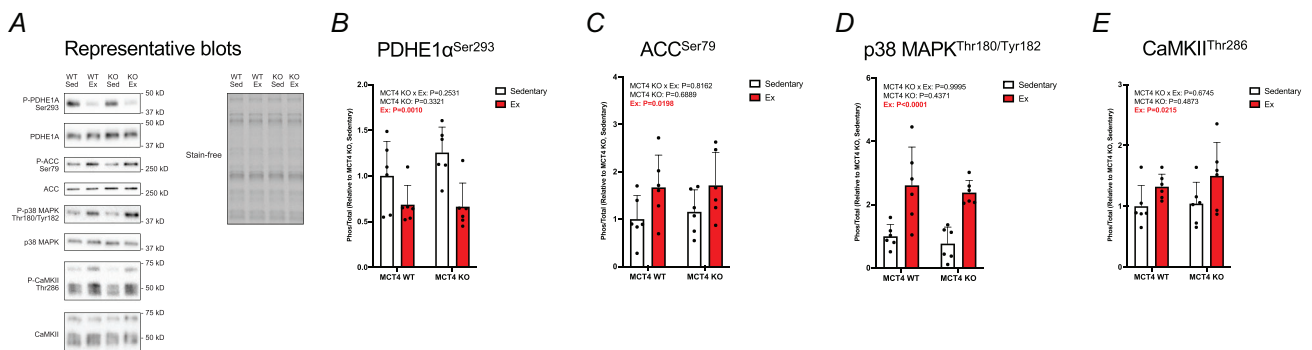
force (Fig. 6C and D). Additionally, we examined twitch characteristics, such as time to onset of contraction, time to peak force and half-relaxation time. HIIT was shown to prolong half-relaxation, but there was no effect of training or MCT4 deficiency on the other measures (Fig. 6E–G). Furthermore, we examined the force–frequency relationship and observed no significant effects of HIIT or MCT4 deficiency (Fig. 6H). Sequential maximal tetanic contractions were performed to assess the rate at which the tension exerted decreased. The fatigue tolerance index was determined by measuring the number of stimuli required to reach 50% of the initial tension (a higher number indicates greater fatigue tolerance). Our findings revealed that a combination of MCT4 deficiency and HIIT significantly enhanced fatigue tolerance compared to other tested conditions (Fig. 6I).

These results indicate that the enhancement of endurance exercise capacity at high intensity by combination of MCT4 deficiency and HIIT are observed both at the organism level as well as at the skeletal muscle tissue level.

**MCT4 knockout and high-intensity interval training additionally or synergistically upregulate activities of rate-limiting and/or irreversible enzymes in glycolysis**

We investigated the physiological basis for the synergistic enhancement of endurance exercise capacity at high intensity from the perspective of bioenergetic adaptations. First, we examined the protein contents of key energy-substrate transporters in the gastrocnemius

**Exercise-responsive signal transduction (Phosphorylation status)**



**Gene expression profiling with RNA-seq**

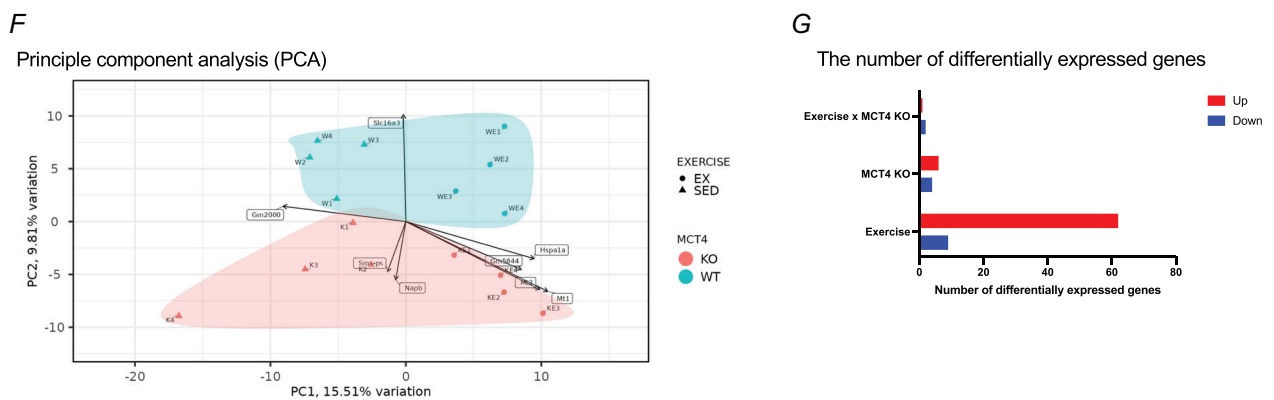


**Figure 4. MCT4 deficiency has little effect on exercise-responsive signal transduction and gene expression changes induced by a single bout of high-intensity interval exercise**  
 A, representative bands of western blot. B–E, phosphorylation status of pyruvate dehydrogenase E1  $\alpha$  (PDHE1 $\alpha$ )<sup>Ser293</sup> (B), acetyl-CoA carboxylase (ACC)<sup>Ser79</sup> (C), p38 mitogen-activated protein kinase (MAPK)<sup>Thr180/Tyr182</sup> (D) and calcium/calmodulin-dependent protein kinase II (CaMKII)<sup>Thr286</sup> (E) in gastrocnemius muscle immediately after exercise. F, principal component analysis processed based on gene expression profiling data in gastrocnemius muscle 3 h after exercise. G, the number of differentially expressed genes with MCT4 deficiency and/or a single bout of high-intensity interval exercise in gastrocnemius muscle 3 h after exercise. Data are expressed as means  $\pm$  SD (MCT4 WT/Sedentary:  $n = 6$ , MCT4 WT/Ex:  $n = 6$ , MCT4 KO/Sedentary:  $n = 6$ , MCT4 KO/Ex:  $n = 6$  for A–E, MCT4 WT/Sedentary:  $n = 4$ , MCT4 WT/Ex:  $n = 4$ , MCT4 KO/Sedentary:  $n = 4$ , MCT4 KO/Ex:  $n = 4$  for F and G). [Colour figure can be viewed at wileyonlinelibrary.com]

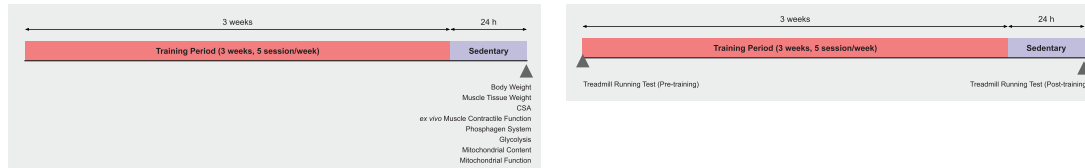
muscle. We found HIIT increased GLUT4 and MCT1 but did not affect FAT/CD36 or MCT4 (Fig. 7A–E). Interestingly, MCT4 deficiency had no significant effect other than on the content of MCT4 protein. These results indicate that adaptations in skeletal muscle transporters cannot account for the synergistically increased endurance exercise capacity at high intensity.

We examined whether MCT4 deficiency and/or HIIT induced adaptations in the following three systems of energy production in skeletal muscle: (1) the phosphagen system, (2) glycolysis and (3) mitochondrial oxidative phosphorylation. First, we measured the activity of creatine kinase and adenylate kinase as the phosphagen system. There were no significant changes in creatine kinase and adenylate kinase activity with either MCT4 deficiency or HIIT (Fig. 8A and B).

Regarding glycolysis, we first examined glycogen concentrations at rest in skeletal muscle. HIIT increased skeletal muscle glycogen stores but was not affected by MCT4 deficiency (Fig. 8C). Subsequently, we measured the activities of the following four enzymes in the rate-limiting and irreversible step of glycolysis: (1) hexokinase (HK), (2) glycogen phosphorylase (GP), (3) phosphofructokinase (PFK) and (4) pyruvate kinase (PK). PFK activity was not significantly affected by either HIIT or MCT4 deficiency (Fig. 8G). The activities of HK and PK were additively increased by HIIT and MCT4 deficiency (Fig. 8D and H). We found that GP activity in the absence of AMP decreased due to HIIT (Fig. 8E). Conversely, GP activity in the presence of AMP (mimicking a state of increased energy demand) was synergistically increased by the combination of MCT4 deficiency and HIIT

## Experimental procedure

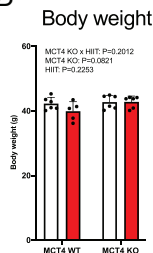
A



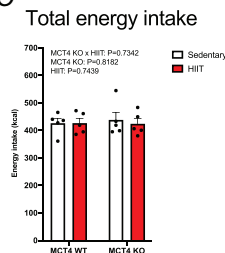
## Body weight and total energy intake

## Muscle weight

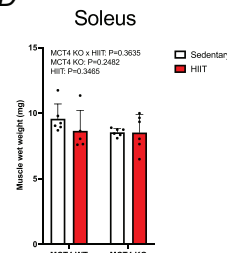
B



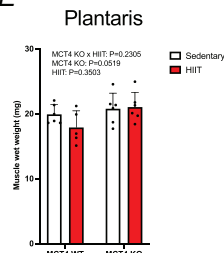
C



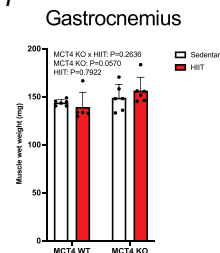
D



E



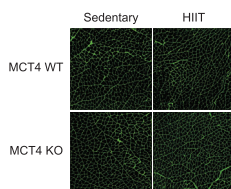
F



## Cross-sectional myofiber area (Gastrocnemius)

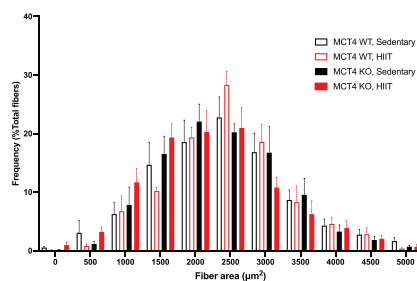
G

Representative image



H

Distribution



I

Mean

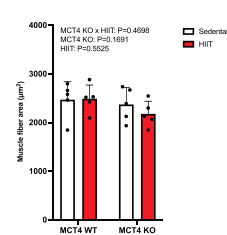


## Figure 5. MCT4 deficiency does not affect skeletal muscle mass and size

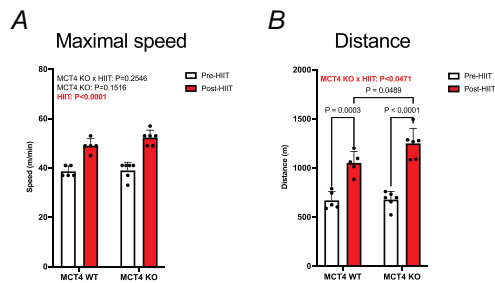
A, experimental procedures for chronic adaptations of 3-week HIIT. B–F, body weight (B), total energy intake (C), muscle weights of soleus (D), plantaris (E) and gastrocnemius (F) after 3-week HIIT intervention. G–I, representative images of cross-sectional myofibre area (G), distribution (H) and mean area (I) after 3-week HIIT intervention in gastrocnemius muscle. Data are expressed as means  $\pm$  SD (MCT4 WT/Sedentary:  $n = 6$ , MCT4 WT/HIIT:  $n = 5$ , MCT4 KO/Sedentary:  $n = 6$ , MCT4 KO/HIIT:  $n = 6$ ). [Colour figure can be viewed at [wileyonlinelibrary.com](http://wileyonlinelibrary.com)]

(Fig. 8F). Finally, we examined lactate dehydrogenase (LDH) activity to evaluate the capacity to bidirectionally convert pyruvate and lactate. The capacity to convert pyruvate to lactate increased with MCT4 deficiency (Fig. 8J). On the other hand, enzymatic activity toward lactate to pyruvate was synergistically upregulated by the combination of MCT4 deficiency and HIIT (Fig. 8J). The changes in LDH activity were not accompanied by any changes in the ratio of lactate dehydrogenase isozymes (Fig. 8K). In summary, it is evident that MCT4 deficiency and HIIT additively and/or synergistically enhance the activity of key enzymes in glycolysis (HK, GP, PK and LDH). These adaptations are interpreted as an increased capacity for ATP and pyruvate/lactate production through glycolysis.

**MCT4 knockout and high-intensity interval training synergistically upregulate the capacity of mitochondrial pyruvate oxidation**

In the context of mitochondrial adaptations, we first examined the adaptation of mitochondrial content. We measured cytochrome *c* oxidase subunit 4 (COX IV) and voltage-dependent anion channel 1 (VDAC) protein levels and the activity of citrate synthase (CS) as biomarkers of mitochondrial content (Fig. 9A–D). We found increases in all of these biomarkers with HIIT, whereas MCT4 deficiency had no effect on any of them (Fig. 9A–D). We subsequently examined whether MCT4 deficiency affects mitochondrial respiratory function. Oxygen consumption rate and ROS production

**Incremental exercise test**



**ex vivo muscle contractile function (EDL)**

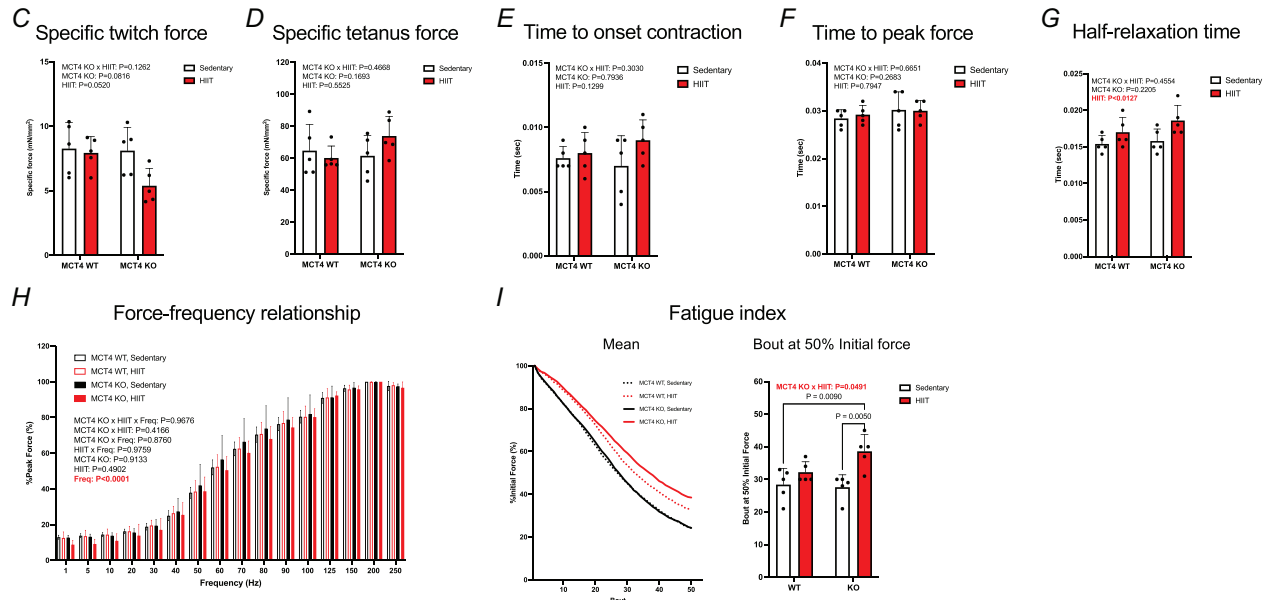


**Figure 6. The combination of MCT4 deficiency and 3 weeks of HIIT synergistically improves endurance exercise capacity**  
 A and B, maximal speed (A) and distance (B) at incremental running test before and after 3-week HIIT. C–I, specific twitch force (C), specific tetanus force (D), time to onset contraction (E), time to peak force (F), half-relaxation time (G), force–frequency relationship (H) and fatigue index (I) in isolated EDL muscle after 3-week HIIT intervention. Data are expressed as means ± SD (MCT4 WT: n = 5, MCT4 KO: n = 5 for A and B, MCT4 WT/Sedentary: n = 5, MCT4 WT/HIIT: n = 5, MCT4 KO/Sedentary: n = 5, MCT4 KO/HIIT: n = 5 for C–I). [Colour figure can be viewed at wileyonlinelibrary.com]

rate were measured in mitochondria isolated/purified from gastrocnemius muscle. The measurements were performed using a combination of four sets of substrates ((1) pyruvate + malate, (2) glutamate + malate, (3) octanoylcarnitine + malate, and (4) succinate + rotenone) and two respiratory states (State 3: ATP synthesis-coupled maximal respiration, and State 2: basal respiration to maintain the electrical gradient of protons). MCT4 deficiency decreased oxygen consumption rate with glutamate + malate (State 3) (Fig. 9F). Oxygen consumption rate with octanoylcarnitine + malate as substrate (States 3 and 2) was increased by HIIT, but was not affected by MCT4 deficiency (Fig. 9G). It is evident that oxygen consumption rate with succinate + rotenone was additively increased by MCT4 deficiency and HIIT in the State 3 condition (Fig. 9H). Interestingly, respiratory capacity under State 3 conditions with pyruvate + malate was synergistically upregulated by the combination of MCT4 deficiency and HIIT (Fig. 9E). ROS production with mitochondrial respiration (a measure of electron leakage in the electron transport chain) broadly supports the results for oxygen consumption rate. Mitochondrial ROS production was reduced under State 3 and State 2 conditions using pyruvate + malate (Fig. 9I). Conversely, MCT4 deficiency enhanced mitochondrial ROS production when glutamate + malate was used as a substrate (Fig. 9J).

In summary, HIIT increases mitochondrial content in skeletal muscle. However, MCT4 deficiency does not affect these volumetric adaptations, though the respiratory function of mitochondria that are increased by HIIT are modified by MCT4 deficiency. In particular, it is notable that respiration coupled to ATP production when

pyruvate + malate is used as a substrate was synergistically enhanced by the combination of MCT4 deficiency and HIIT.

### MCT4 knockout and high-intensity interval training synergistically increase pyruvate dehydrogenase complex activity

We then aimed to understand the potential physiological basis underlying the increase in the mitochondrial oxidative capacity of pyruvate by the combination of MCT4 deficiency and HIIT. The initial steps in pyruvate oxidation are as follows: pyruvate produced in the cytosol is transported to the mitochondrial matrix through mitochondrial pyruvate carriers (MPCs) localized on the mitochondrial inner membrane. Pyruvate is then converted to acetyl-CoA by the pyruvate dehydrogenase complex (PDHc). Based on the above physiological background, we examined the protein levels of MPCs and the activity of PDHc in the isolated mitochondrial fraction. HIIT increased the content of MPC2, but not MPC1 (Fig. 10A–C). On the other hand, MCT4 deficiency did not affect either protein contents. Interestingly, the combination of HIIT and MCT4 deficiency synergistically increased PDHc activity (Fig. 10D).

To elucidate the factors responsible for the increased activity of PDHc by MCT4 knockout and HIIT, we then examined the protein content of the component of PDHc and the phosphorylation status of regulatory subunit (PDHE1 $\alpha$ ). The protein levels of PDHE1 $\alpha$ , dihydrolipoamide S-acetyltransferase (DLAT) and dihydrolipoamide dehydrogenase (DLD) were examined

### Substrate transporters

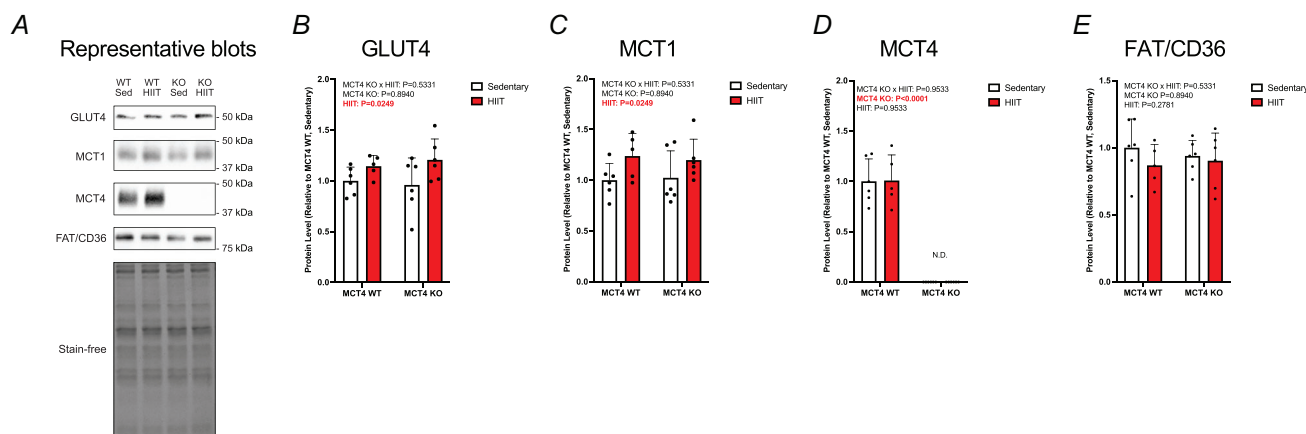


### Figure 7. MCT4 deficiency has little effect on substrate transporters

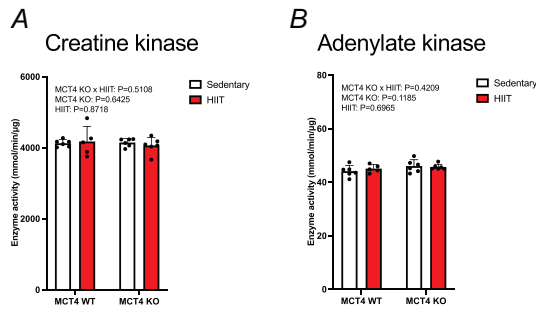
A, representative bands of western blot. B–E, protein contents of glucose transporter 4 (GLUT4) (B), MCT1 (C), MCT4 (D) and FAT/CD36 (E) in gastrocnemius muscle after 3-week HIIT intervention. Data are expressed as means  $\pm$  SD (MCT4 WT/Sedentary:  $n = 6$ , MCT4 WT/HIIT:  $n = 5$ , MCT4 KO/Sedentary:  $n = 6$ , MCT4 KO/HIIT:  $n = 6$ ). [Colour figure can be viewed at [wileyonlinelibrary.com](http://wileyonlinelibrary.com)]

as subunits constituting PDHc. We found that HIIT and MCT4 additively increased the content of PDHE1 $\alpha$ , and synergistically increased DLAT, respectively (Fig. 10E–G). The activity of PDHc is regulated by phosphorylation of the PDHE1 $\alpha$  subunit. As described above, both MCT4 deficiency and HIIT additively increased the total content of the PDHE1 $\alpha$  subunit (Fig. 10F). However, the level of phosphorylated PDHE1 $\alpha$  at Ser293 (inactive form) was not affected by MCT4 deficiency or HIIT (Fig. 10I). These data are interpreted as an increase in the active PDHE1 $\alpha$  form with the combination of MCT4 deficiency and HIIT. We then examined the protein levels regulating

the phosphorylation state of PDHE1 $\alpha$ . It was found that pyruvate dehydrogenase kinase (PDK) 2 and PDK4, both of which phosphorylate PDHE1 $\alpha$ , were increased by HIIT with no significant effects of MCT4 deficiency (Fig. 10E, J and K). On the contrary, the protein level of PDP1, the protein which dephosphorylates PDHE1 $\alpha$ , was synergistically increased by MCT4 deficiency and HIIT (Fig. 10L).

To summarize the adaptations of the initial steps of pyruvate oxidation, it is evident that the combination of MCT4 deficiency and HIIT increases the activity of PDHc, which converts pyruvate to acetyl-CoA. In addition, this

**Phosphagen system**



**Glycolysis and lactate metabolism**

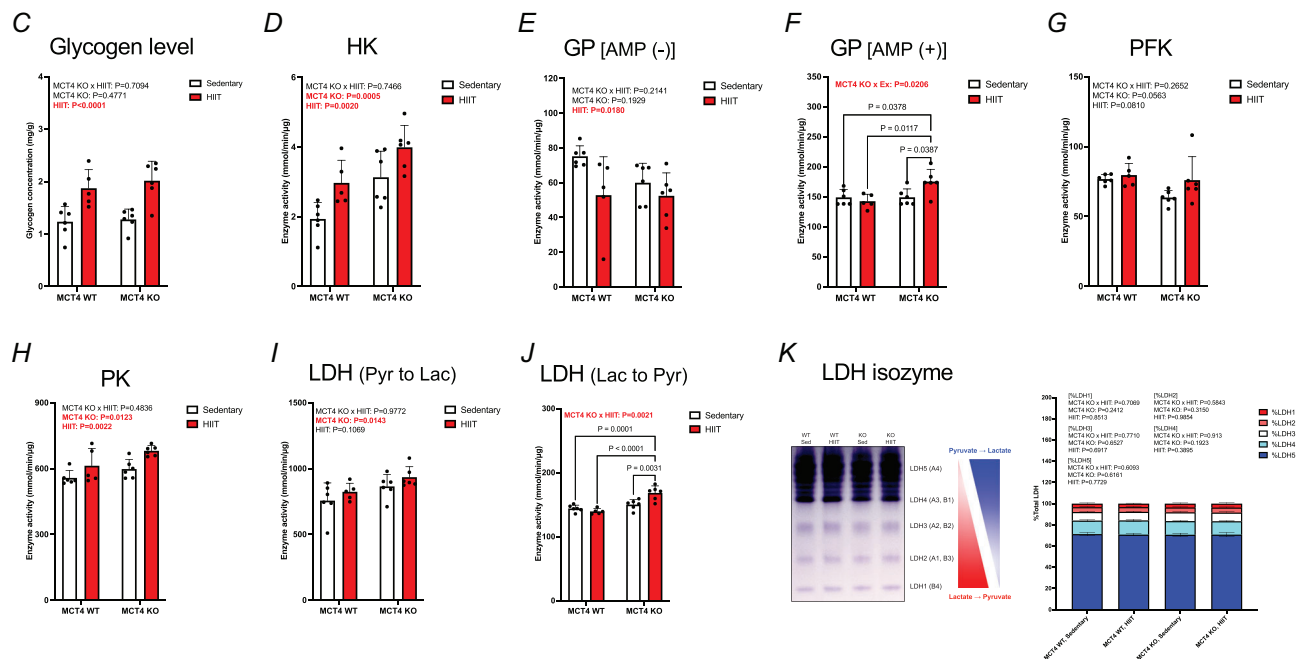


**Figure 8. The combination of MCT4 deficiency and 3 weeks of HIIT additively or synergistically increases glycolytic enzyme activities**

A and B, creatine kinase activity (A) and adenylate kinase activity (B) in gastrocnemius muscle after 3-week HIIT intervention. C–K, glycogen concentration (C), hexokinase (HK) activity (D), glycogen phosphorylase (GP) activity without AMP (E), GP activity with AMP (F), phosphofructokinase (PFK) activity (G), pyruvate kinase (PK) activity (H), lactate dehydrogenase (LDH) activity (pyruvate to lactate) (I), LDH activity (lactate to pyruvate) (J) and LDH isozymes (K) after 3-week HIIT intervention. Data are expressed as means  $\pm$  SD (MCT4 WT/Sedentary: n = 6, MCT4 WT/HIIT: n = 5, MCT4 KO/Sedentary: n = 6, MCT4 KO/HIIT: n = 6). [Colour figure can be viewed at [wileyonlinelibrary.com](http://wileyonlinelibrary.com)]

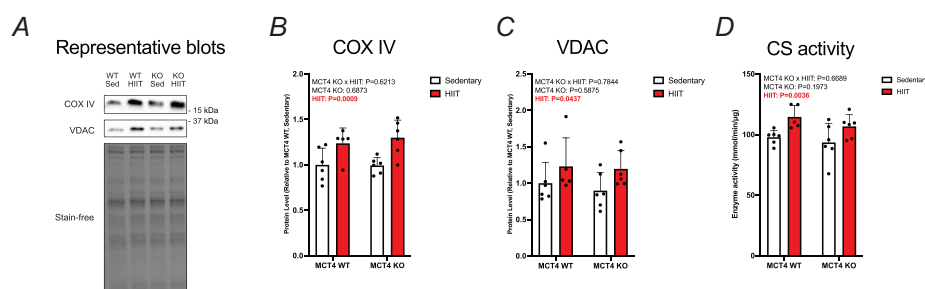
adaptation is paralleled by an increase in the components of the PDHC, and an increase in the active form of the regulatory subunit.

### MCT4 knockout and high-intensity interval training enhances rate-limiting enzyme activities at TCA cycle and electron transport chain

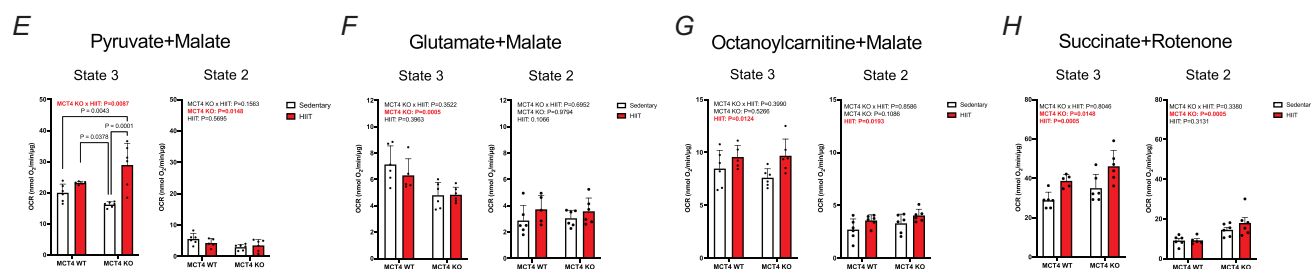
We subsequently examined effects of MCT4 deficiency and HIIT on enzymatic activities of the TCA cycle and electron transport chain in isolated mitochondria. We defined enzymes responsible for rate-limiting or irreversible reactions or for supplying NADH or FADH<sub>2</sub> in the TCA cycle as key enzymes for our analysis.

We found that HIIT and MCT4 deficiency additively increased the activity of isocitrate dehydrogenase (the rate-limiting enzyme of the TCA cycle) but not citrate synthase,  $\alpha$ -ketoglutarate dehydrogenase, and malate dehydrogenase (Fig. 11A–E). We subsequently measured the enzymatic activities of the electron transport chain. Contrary to our expectation, the complex I-related enzyme activities (complex I and I + III) were decreased by MCT4 deficiency (Fig. 11F and G). On the other hand, the enzymatic activity of complex IV, the rate-limiting step of the electron transport chain, was additively increased by HIIT and MCT4 deficiency (Fig. 11I). The enhanced formation of respiratory chain supercomplexes contributes to smoother electron transport, leading to higher rates of oxygen consumption and lower rates

#### Mitochondrial content



#### Mitochondrial oxygen consumption rate (isolated mitochondria)



#### Mitochondrial ROS emission rate (isolated mitochondria)

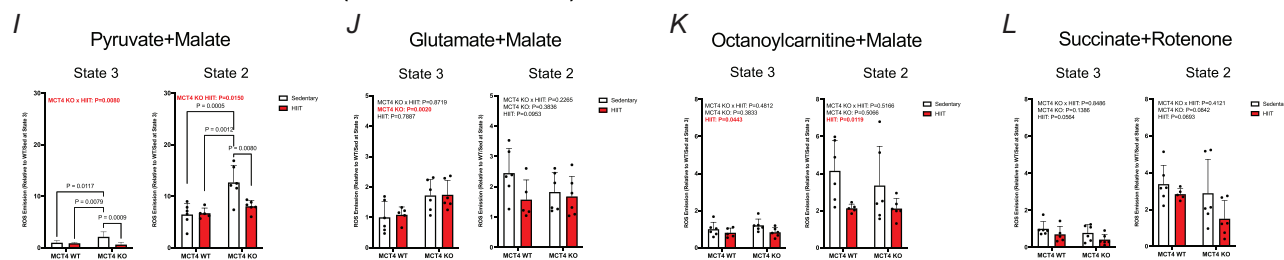


**Figure 9. The combination of MCT4 deficiency and 3 weeks of HIIT synergistically increases mitochondrial pyruvate oxidation capacity**

A, representative bands of western blot. B–D, protein contents of cytochrome c oxidase subunit IV (COXIV) (B), voltage-dependent anion channel (VDAC) (C) and citrate synthase (CS) (D) activity in gastrocnemius muscle after 3-week HIIT intervention. E–H, oxygen consumption rate measured with pyruvate + malate (E), glutamate + malate (F), octanoylcarnitine + malate (G) and succinate + rotenone (H) in mitochondrial fraction purified from gastrocnemius muscle after 3-week HIIT intervention. I–L, ROS emission rate measured with pyruvate + malate (I), glutamate + malate (J), octanoylcarnitine + malate (K) and succinate + rotenone (L) in mitochondrial fraction purified from gastrocnemius muscle after 3-week HIIT intervention. Data are expressed as means  $\pm$  SD (MCT4 WT/Sedentary:  $n = 6$ , MCT4 WT/HIIT:  $n = 5$ , MCT4 KO/Sedentary:  $n = 6$ , MCT4 KO/HIIT:  $n = 6$ ). [Colour figure can be viewed at [wileyonlinelibrary.com](http://wileyonlinelibrary.com)]

of ROS production (Greggio et al., 2017; Heden et al., 2019). Therefore, we examined whether the improved mitochondrial oxidative capacity by the combination of MCT4 deficiency and HIIT was accompanied by enhanced physical interactions between the respiratory chains. However, we did not detect significant changes in respiratory supercomplex formation with MCT4 deficiency or HIIT (Fig. 11J–M).

To summarize the adaptations of activities of key mitochondrial enzymes, we found that the combination of MCT4 deficiency and HIIT additively enhances the rate-limiting enzymes in TCA cycle (isocitrate

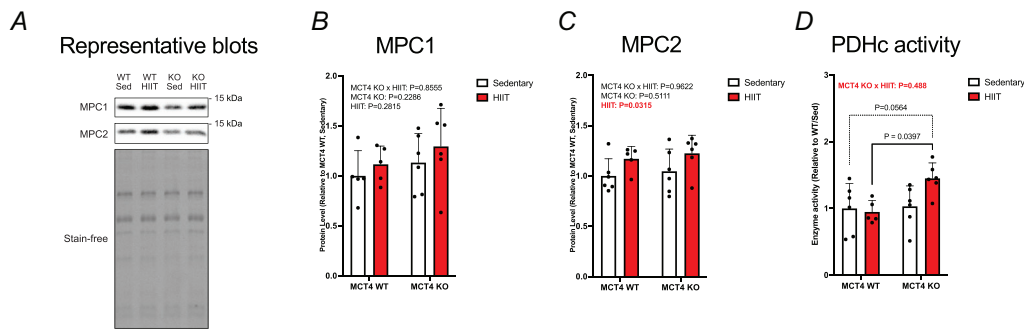
dehydrogenase) and electron transport chain (complex IV).

## Discussion

### Development of a novel line of MCT4 knockout mice

Advancements in CRISPR/Cas9 technology have expanded the horizons of genetically modified organisms, moving beyond the confines of traditional model species to now include non-model animals and strains (Dickinson et al., 2020; Imai et al., 2022; Mendoza & Trinh, 2018).

### Pyruvate oxidation pathway (isolated mitochondria)



### Component and regulatory factors of pyruvate dehydrogenase complex (isolated mitochondria)

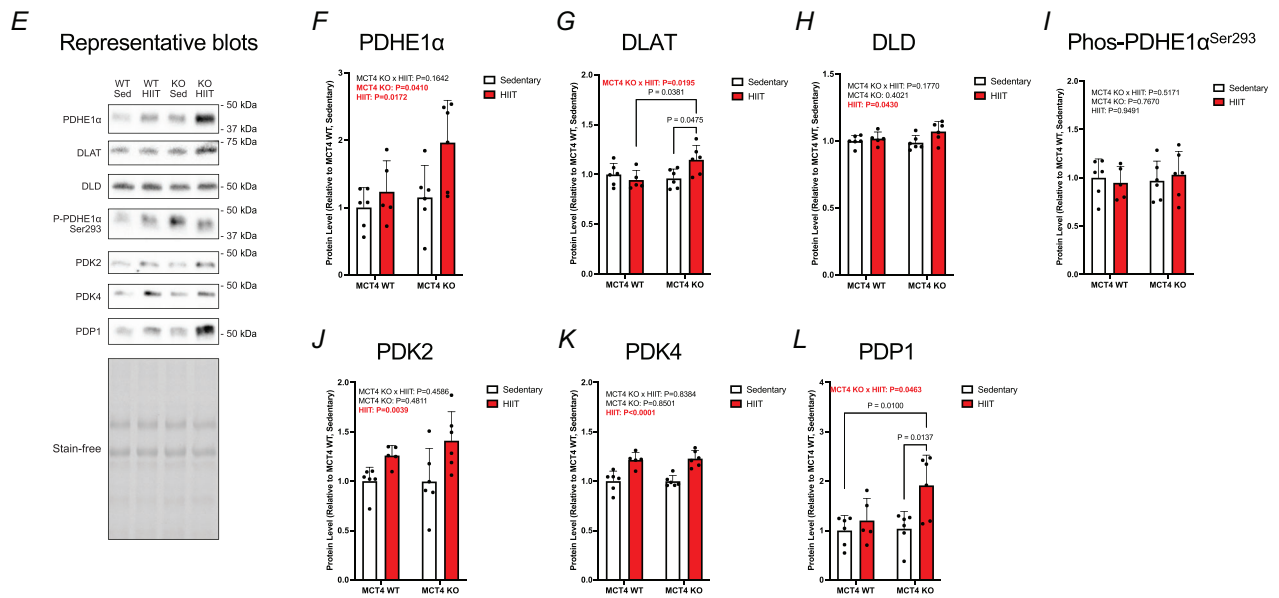


**Figure 10. The combination of MCT4 deficiency and 3 weeks of HIIT synergistically increases pyruvate dehydrogenase complex activity**

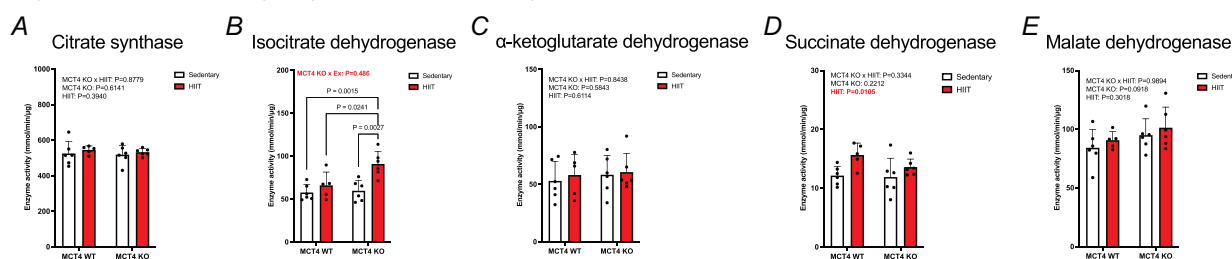
A, representative bands of western blot. B–D, protein contents of mitochondrial pyruvate carrier (MPC)1 (B), MPC2 (C) and pyruvate dehydrogenase complex (PDHC) activity (D) in mitochondrial fraction purified from gastrocnemius muscle after 3-week HIIT intervention. E, representative bands of western blot. F–L, protein contents of pyruvate dehydrogenase E1 alpha (PDHE1α) subunit (F), dihydrolipoamide S-acetyltransferase (DLAT) (G), dihydrolipoamide dehydrogenase (DLD) (H), phosphorylated PDHE1α<sup>Ser293</sup> (I), pyruvate dehydrogenase kinase (PDK) 2 (J), PDK4 (K) and pyruvate dehydrogenase phosphatases (PDP) 1 (L) in mitochondrial fraction purified from gastrocnemius muscle after 3-week HIIT intervention. Data are expressed as means ± SD (MCT4 WT/Sedentary: n = 6, MCT4 WT/HIIT: n = 5, MCT4 KO/Sedentary: n = 6, MCT4 KO/HIIT: n = 6). [Colour figure can be viewed at wileyonlinelibrary.com]

Such breakthroughs allow researchers to scrutinize gene functions in animal species and strains that are more aligned with their research objectives. In our case, creating MCT4-deficient mice in a strain primed for high-intensity exercise granted us the opportunity to investigate the combined effects of high-intensity exercise/training and MCT4 deficiency. Numerous reverse genetics studies have recently underscored the diverse responses and adaptations elicited by gene deletion or overexpression across distinct species and strains (Ebihara et al., 2015; Gu et al., 2016; Mashimo et al., 2012; Nakamura et al., 2014). As discussed below, our study aligns with this narrative, and the single effect of MCT4 deficiency may be interactively modified by genetic background and other genetic mutations. Positioned in this context, our

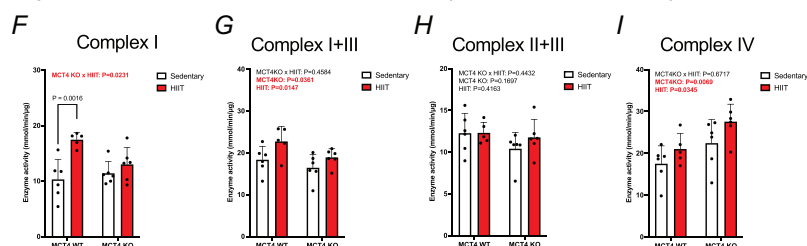
study also amplifies the importance of investigating gene functions across a broad spectrum of animal species and strains, underscoring its pertinence in skeletal muscle exercise physiology.

Our research indicates that MCT4 deficiency and further accumulations of lactate within skeletal muscle does not result in any decrease in exercise and contractile performances, as demonstrated by the incremental exercise tests and *ex vivo* muscle contractile function assays, respectively. These findings clearly demonstrated again that lactate accumulation in skeletal muscle is not the primary cause of fatigue. However, our results contrast with those from a previous study which reported that MCT4-deficient mice of the C57BL/6NTac strain background exhibit reduced exercise capacity at the organismal

### Enzyme activities in TCA cycle (isolated mitochondria)



### Enzyme activities in electron transport chain (isolated mitochondria)



### Respiratory chain supercomplex

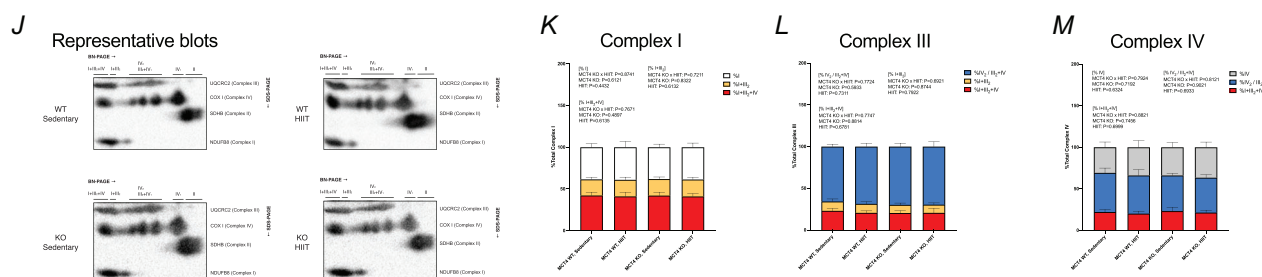


### Figure 11. The combination of MCT4 deficiency and 3 weeks of HIIT additionally or synergistically increases rate-limiting enzymes in TCA cycle and electron transport chain

A–E, citrate synthase activity (A), isocitrate dehydrogenase activity (B),  $\alpha$ -ketoglutarate dehydrogenase activity (C), succinate dehydrogenase activity (= complex II activity) (D) and malate dehydrogenase activity (E) in mitochondrial fraction purified from gastrocnemius muscle after 3-week HIIT intervention. F–I, complex I activity (F), complex I + III activity (G), complex II + III activity (H) and complex IV activity (I) in mitochondrial fraction purified from gastrocnemius muscle after 3-week HIIT intervention. J–M, representative images of supercomplex assay (J), percentage of complex I (K), complex III (L) and complex IV (M) in each supercomplex in mitochondrial fraction purified from gastrocnemius muscle after 3-week HIIT intervention. Data are expressed as means  $\pm$  SD (MCT4 WT/Sedentary:  $n = 6$ , MCT4 WT/HIIT:  $n = 5$ , MCT4 KO/Sedentary:  $n = 6$ , MCT4 KO/HIIT:  $n = 6$ ). [Colour figure can be viewed at [wileyonlinelibrary.com](http://wileyonlinelibrary.com)]

level (during treadmill running and spontaneous wheel cage activity), while their isolated muscle contractile performance remains unaffected (Bisetto et al., 2019). This discrepancy may be attributed to the differing genetic backgrounds of the MCT4-deficient mice used in each study. The C57BL/6 strain, which is commonly used as the genetic background for genetically modified mice, is known to have an inactive mutation in the *Cox7a2l* gene involved in the assembly of mitochondrial super-complexes (Lapiente-Brun et al., 2013). Additionally, the C57BL/6NTac substrain carries a mutation in the genes involved in immunology and retinal degeneration (Concas et al., 2017). Therefore, when discussing the differences in results between previous studies and the present study, it may be necessary to at least consider the interaction between the function of these genes and the function of MCT4.

The administration of exogenous sodium lactate to cultured cells and experimental animals has long been a prevalent method to investigate the role of lactate as an energy substrate and a signalling molecule in the circulation. However, recent studies have highlighted that some of the physiological adaptations attributed to exogenous sodium lactate might actually stem from sodium-induced osmotic changes, rather than lactate itself (Lund et al., 2023). This crucial insight emphasizes the limitations of relying solely on exogenous lactate administration for a thorough understanding of lactate-mediated inter-organ communication. Consequently, alternative approaches, such as inhibiting endogenous lactate transport, are vital to gain a more complete perspective. In this vein, utilizing MCT4-deficient mice developed in this study represents a pivotal strategy to explore lactate's role in inter-organ crosstalk under more physiological conditions. Moving forward, our research aims to expand its scope beyond skeletal muscle to encompass lactate-recipient organs, including the liver, adipose tissue, heart and brain. This broader approach is expected to provide a more comprehensive understanding of lactate metabolism during exercise.

### The synergistic effects of high-intensity interval training and MCT4 deficiency on metabolic remodelling and exercise capacity

The primary aim of this study was to investigate how MCT4 deficiency affects skeletal muscle adaptations to HIIT. Our most significant finding was that the combination of MCT4 deficiency and HIIT enhanced endurance exercise capacity at high intensities. To elucidate the physiological mechanisms underlying these adaptations, we conducted an extensive examination of the activities of the enzymes, protein complexes

and organelles involved in energy metabolism. We focused on assessing enzyme activity rather than simply measuring protein contents, as it provides a more physiologically meaningful context by incorporating the effects of post-translational modifications and protein-protein interactions. Our results revealed that MCT4 deficiency and HIIT collectively enhanced 'glucose catabolism' processes, such as the activities of rate-limiting enzymes in glycolysis and increased the mitochondrial capacity to oxidize pyruvate. Given that glucose and/or glycogen is the primary energy source during high-intensity exercise, these findings partially explain the enhanced exercise capacity observed during high-intensity exercise.

Interestingly, the observed increase in pyruvate oxidation capacity in MCT4-deficient mice was a functional improvement per unit mitochondrion, whereas MCT4 deficiency did not affect the training-induced increase in mitochondrial contents. Yamada et al. recently reported that both low-frequency (mimicking low-intensity exercise) and high-frequency (mimicking high-intensity exercise) electrical stimulation induced similar increases in mitochondrial content (Yamada et al., 2021). However, only high-frequency pulses led to an increase in the oxidative capacity of pyruvate in isolated mitochondria. Similar findings have been reported in human studies, where exercise intensity was found to influence mitochondrial function, but not content (Granata et al., 2016). Integrating the present findings with these previous studies suggests that the mitochondrial functional adaptations specific to high-intensity exercise training are similar to those provided by the combination of MCT4 deficiency and HIIT. Therefore, the enhanced accumulation of lactate in skeletal muscle might be integral to the functional adaptation of mitochondria in skeletal muscle induced by high-intensity exercise and training.

Contrarily, it remains unclear whether reducing lactate accumulation during exercise would result in adaptations opposite to those observed in this study. Hoshino and colleagues reported that decreasing lactate accumulation in skeletal muscle during exercise by increasing pyruvate oxidation with dichloroacetate (DCA) attenuates HIIT-induced increases in mitochondrial content, glycogen and fatty acid transporter (FAT/CD36) levels (Hoshino et al., 2015). In our study, increased lactate accumulation due to MCT4 deficiency had no effect on mitochondrial content, glycogen levels or FAT/CD36 protein levels. However, the impact of reduced lactate accumulation on skeletal muscle exercise capacity, activity of enzymes in the glycolytic system or adaptations in mitochondrial respiratory function has not been examined in previous studies using DCA. Thus, while it is currently impossible to draw definitive conclusions, it seems plausible that skeletal muscle adaptations resulting from increased or decreased lactate

concentration might not necessarily yield diametrically opposed outcomes. Further research is needed to understand the relationship between lactate metabolism and exercise-induced adaptations in skeletal muscle.

Recently, lactylation has been identified as a new post-translational modification of proteins using lactate as a substrate (Zhang et al., 2019). Lactylation of histone H3 at Lys27 has been shown to epigenetically promote gene transcription (Zhang et al., 2019). We initially hypothesized that increased lactate accumulation during exercise due to MCT4 deficiency might enhance the gene expression response to exercise, possibly via histone lactylation. However, we were unable to validate commercially available anti-lactylated histone antibodies satisfactorily, and therefore could not investigate whether histone lactylation is enhanced in MCT4 deficiency in the present study. Nevertheless, from a more physiologically relevant perspective, we profiled gene expression changes in skeletal muscle 3 h post-exercise and found that the synergistic effects of MCT4 deficiency and high-intensity interval exercise were minimal. Therefore, within the context of high-intensity exercise, the potential influence of MCT4 deficiency on histone lactylation may not be a primary concern. Long-term adaptations of skeletal muscle to training are typically attributed to the accumulation of intracellular signalling responses and gene expression changes following each exercise session. However, our study showed that long-term adaptations (protein expression and enzyme activity) and initial/early responses (gene expression changes) to the combination of MCT4 deficiency and HIIT do not always align. This discrepancy suggests that enhanced lactate accumulation due to MCT4 deficiency may impact post-transcriptional processes. Lactylation has also been identified in proteins other than histone H3 (Huang et al., 2023; Maschari et al., 2022; Yang et al., 2023), suggesting that such post-translational modifications might contribute to long-term metabolic adaptations. However, our current study could not determine how lactate within skeletal muscle cells enhances metabolic adaptation to HIIT. This matter needs further investigation in future research.

### Could MCT4 deficiency enhance metabolic acidosis?

MCT4 serves as a crucial co-transporter of lactate and protons. This suggests that MCT4 deficiency may exacerbate metabolic acidosis (not lactic acidosis). Experimentally induced acidosis has been observed to influence a range of biological processes, either directly or indirectly (Visser et al., 2023). Consequently, comprehending the effects of MCT4 deficiency on intracellular pH and its subsequent biological consequences is vital for interpreting our findings. Our study does not directly measure pH, precluding definitive conclusions on the enhancement of metabolic acidosis due to

MCT4 deficiency and its interaction with exercise. Cells employ various pH buffering systems to maintain intracellular pH stability, including proton extrusion mechanisms like MCTs, enzymatic reactions consuming protons and processes related to mitochondrial oxidative phosphorylation (Robergs et al., 2004). We hypothesized that MCT1 may partially compensate for the acidosis induced by MCT4 deficiency. This compensation is functional rather than an upregulation in MCT1 expression. In the present study, we observed that blood lactate concentrations increased up to about 7 mmol/l in MCT4-deficient mice during a progressive exercise stress test. Our observations indicate that MCT4 deficiency does not fully preclude lactate release during exercise. This suggests that while MCT4 plays a significant role in lactate and proton transport, its absence does not completely halt lactate and proton efflux from muscle cells. Although MCT1 is sometimes described as contributing to lactate influx, MCT1 is a transporter that transports lactate and hydrogen ions only according to a concentration gradient and not in a specific direction of transport. Given MCT1's affinity for lactate ( $K_m$ : 17–34 mM for MCT4 and 3.5 mM for MCT1) and 10 times higher intracellular proton concentration compared to the extracellular compartment, it likely facilitates lactate and proton release into the circulation at the onset of exercise and during low-to-moderate intensity exercise (Halestrap, 2013; Juel, 2008). Chatel and coworkers have shown that heterozygous loss of MCT1 results in a further decrease in pH immediately after the onset of skeletal muscle contraction (~1 min) compared to wild type (Chatel et al., 2017). This observation at least partially supports our inference that MCT1-mediated lactate and proton release partially compensates for the effects of MCT4 deficiency. On the other hand, the study have also shown that heterozygous loss of MCT1 results in increased pH in resting skeletal muscle and altered expression of carbonic anhydrase II (CAII), one of the enzymes that regulate pH (Chatel et al., 2017). These findings illustrate that it is difficult to extrapolate the properties of a single or small number of molecules directly to intracellular physiology and again suggest that the regulatory mechanisms of intracellular pH are complex. Therefore, to fully understand MCT4 deficiency's impact on pH, a comprehensive evaluation is necessary for a holistic conclusion. Future experimental investigations addressing these questions would not only build upon the findings of this study but also contribute new insights into the longstanding debate over skeletal muscle pH and its effect on muscle function.

### Conclusion

This study was undertaken to examine whether further elevated lactate accumulation in skeletal muscle influences its adaptation to exercise and training. We developed

MCT4-deficient mice with a genetic background of the Jcl:ICR strain and conducted these mice to high-intensity interval exercise and training. Our findings reveal that MCT4 deficiency, in combination with HIIT, significantly enhances endurance exercise capacity at high intensity. This physiological adaptation is underpinned by an enhanced capacity of the glycolysis and an increased mitochondrial respiratory capacity of pyruvate. Our findings contribute to a deeper understanding of the crucial role of lactate accumulation in high-intensity exercise and adaptations. Further research is warranted to elucidate the molecular mechanisms underlying these adaptations, which could potentially be exploited to further optimize exercise training programs.

## References

- Bisetto, S., Wright, M. C., Nowak, R. A., Lepore, A. C., Khurana, T. S., Loro, E., & Philp, N. J. (2019). New insights into the lactate shuttle: Role of MCT4 in the modulation of the exercise capacity. *iscience*, **22**, 507–518.
- Bonen, A. (2001). The expression of lactate transporters (MCT1 and MCT4) in heart and muscle. *European Journal of Applied Physiology*, **86**(1), 6–11.
- Bröer, S., Schneider, H.-P., Bröer, A., Rahman, B., Hamprecht, B., & Deitmer, J. W. (1998). Characterization of the monocarboxylate transporter 1 expressed in *Xenopus laevis* oocytes by changes in cytosolic pH. *Biochemical Journal*, **333**(1), 167–174.
- Brooks, G. A. (1986). The lactate shuttle during exercise and recovery. *Medicine and Science in Sports and Exercise*, **18**(3), 360–368.
- Brooks, G. A. (2000). Intra- and extra-cellular lactate shuttles. *Medicine and Science in Sports and Exercise*, **32**(4), 790–799.
- Brooks, G. A. (2018). The science and translation of lactate shuttle theory. *Cell Metabolism*, **27**(4), 757–785.
- Brooks, G. A. (2020). Lactate as a fulcrum of metabolism. *Redox Biology*, **35**, 101454.
- Cairns, S. P. (2006). Lactic acid and exercise performance: Culprit or friend? *Sports Medicine*, **36**(4), 279–291.
- Carrière, A., Jeanson, Y., Berger-Müller, S., André, M., Chenouard, V., Arnaud, E., Barreau, C., Walther, R., Galinier, A., Wdziekonski, B., Villageois, P., Louche, K., Collas, P., Moro, C., Dani, C., Villarroya, F., & Casteilla, L. (2014). Browning of white adipose cells by intermediate metabolites: An adaptive mechanism to alleviate redox pressure. *Diabetes*, **63**(10), 3253–3265.
- Chatel, B., Bendahan, D., Hourdé, C., Pellerin, L., Lengacher, S., Magistretti, P., Le Fur, Y., Vilmen, C., Bernard, M., & Messonnier, L. A. (2017). Role of MCT1 and CAII in skeletal muscle pH homeostasis, energetics, and function: In vivo insights from MCT1 haploinsufficient mice. *Federation of American Societies for Experimental Biology Journal*, **31**(6), 2562–2575.
- Concas, D., Cater, H., & Wells, S. (2017). A scoring system for the evaluation of the mutated *Crb1*/rd8-derived retinal lesions in C57BL/6N mice. *FI000Res*, **6**, 404.
- Dickinson, M. H., Vosshall, L. B., & Dow, J. A. T. (2020). Genome editing in non-model organisms opens new horizons for comparative physiology ed. Dickinson MH, Vosshall LB & Dow JAT. *Journal of Experimental Biology*, **223**, (Pt Suppl 1), jeb221119.
- Dimmer, K.-S., Friedrich, B., Lang, F., Deitmer, J. W., & Bröer, S. (2000). The low-affinity monocarboxylate transporter MCT4 is adapted to the export of lactate in highly glycolytic cells. *Biochemical Journal*, **350**(1), 219.
- Dubouchaud, H., Butterfield, G. E., Wolfel, E. E., Bergman, B. C., & Brooks, G. A. (2000). Endurance training, expression, and physiology of LDH, MCT1, and MCT4 in human skeletal muscle. *American Journal of Physiology-Endocrinology and Metabolism*, **278**(4), E571–E579.
- Ebihara, C., Ebihara, K., Aizawa-Abe, M., Mashimo, T., Tomita, T., Zhao, M., Gumbilai, V., Kusakabe, T., Yamamoto, Y., Aotani, D., Yamamoto-Kataoka, S., Sakai, T., Hosoda, K., Serikawa, T., & Nakao, K. (2015). Seipin is necessary for normal brain development and spermatogenesis in addition to adipogenesis. *Human Molecular Genetics*, **24**(15), 4238–4249.
- Egan, B., Carson, B. P., Garcia-Roves, P. M., Chibalin, A. V., Sarsfield, F. M., Barron, N., Mccaffrey, N., Moyna, N. M., Zierath, J. R., & O'gorman, D. J. (2010). Exercise intensity-dependent regulation of peroxisome proliferator-activated receptor  $\gamma$  coactivator-1 $\alpha$  mRNA abundance is associated with differential activation of upstream signalling kinases in human skeletal muscle. *The Journal of Physiology*, **588**(10), 1779–1790.
- Garcia, C. K., Goldstein, J. L., Pathak, R. K., Anderson, R. G. W., & Brown, M. S. (1994). Molecular characterization of a membrane transporter for lactate, pyruvate, and other monocarboxylates: Implications for the Cori cycle. *Cell*, **76**(5), 865–873.
- Ge, S. X., Son, E. W., & Yao, R. (2018). iDEP: An integrated web application for differential expression and pathway analysis of RNA-Seq data. *BMC Bioinformatics*, **19**(1), 534.
- Granata, C., Oliveira, R. S. F., Little, J. P., Renner, K., & Bishop, D. J. (2016). Training intensity modulates changes in PGC-1 $\alpha$  and p53 protein content and mitochondrial respiration, but not markers of mitochondrial content in human skeletal muscle. *The Federation of American Societies for Experimental Biology Journal*, **30**(2), 959–970.
- Greggio, C., Jha, P., Kulkarni, S. S., Lagarrigue, S., Broskey, N. T., Boutant, M., Wang, X.u, Conde Alonso, S., Ofori, E., Auwerx, J., Cantó, C., & Amati, F. (2017). Enhanced respiratory chain supercomplex formation in response to exercise in human skeletal muscle. *Cell Metabolism*, **25**(2), 301–311.
- Gu, H., Cao, Y., Qiu, B., Zhou, Z., Deng, R., Chen, Z., Li, R., Li, X., Wei, Q., Xia, X., & Yong, W. (2016). Establishment and phenotypic analysis of an *Mstn* knockout rat. *Biochemical and Biophysical Research Communications*, **477**(1), 115–122.
- Halestrap, A. P. (2013). Monocarboxylic acid transport. *Comprehensive physiology*, **3**(4), 1611–1643.

- Hashimoto, T., Hussien, R., Oommen, S., Gohil, K., & Brooks, G. A. (2007). Lactate sensitive transcription factor network in L6 cells: Activation of MCT1 and mitochondrial biogenesis. *The Federation of American Societies for Experimental Biology Journal*, **21**(10), 2602–2612.
- Heden, T. D., Johnson, J. M., Ferrara, P. J., Eshima, H., Verkerke, A. R. P., Wentzler, E. J., Siripoksup, P., Narowski, T. M., Coleman, C. B., Lin, C.-T.e, Ryan, T. E., Reidy, P. T., De Castro Brás, L. E., Karner, C. M., Burant, C. F., Maschek, J. A., Cox, J. E., Mashek, D. G., Kardon, G., Boudina, S., Zeczycy, T. N., Rutter, J., Shaikh, S. R., Vance, J. E., Drummond, M. J., Neuffer, P. D., & Funai, K. (2019). Mitochondrial PE potentiates respiratory enzymes to amplify skeletal muscle aerobic capacity. *Science Advances*, **5**(9), eaax8352.
- Hoshino, D., Tamura, Y., Masuda, H., Matsunaga, Y., & Hatta, H. (2015). Effects of decreased lactate accumulation after dichloroacetate administration on exercise training-induced mitochondrial adaptations in mouse skeletal muscle. *Physiological Reports*, **3**(9), e12555.
- Hoxhaj, G., Hughes-Hallett, J., Timson, R. C., Ilagan, E., Yuan, M., Asara, J. M., Ben-Sahra, I., & Manning, B. D. (2017). The mTORC1 Signaling Network Senses Changes in Cellular Purine Nucleotide Levels. *Cell Reports*, **21**(5), 1331–1346.
- Huang, W., Su, J., Chen, X., Li, Y., Xing, Z., Guo, L., Li, S., & Zhang, J. (2023). High-intensity interval training induces protein lactylation in different tissues of mice with specificity and time dependence. *Metabolites*, **13**(5), 647.
- Imai, Y., Tanave, A., Matsuyama, M., & Koide, T. (2022). Efficient genome editing in wild strains of mice using the i-GONAD method. *Scientific Reports*, **12**(1), 13821.
- Juel, C. (2008). Regulation of pH in human skeletal muscle: Adaptations to physical activity. *Acta Physiologica*, **193**(1), 17–24.
- Kasai, A., Jee, E., Tamura, Y., Kouzaki, K., Kotani, T., & Nakazato, K. (2022). Aldehyde dehydrogenase 2 deficiency promotes skeletal muscle atrophy in aged mice. *American Journal of Physiology-Regulatory, Integrative and Comparative Physiology*, **322**(6), R511–R525.
- Kitaoka, Y.u, Takeda, K., Tamura, Y., & Hatta, H. (2016). Lactate administration increases mRNA expression of PGC-1 $\alpha$  and UCP3 in mouse skeletal muscle. *Applied Physiology, Nutrition, and Metabolism*, **41**(6), 695–698.
- Kotani, T., Takegaki, J., Takagi, R., Nakazato, K., & Ishii, N. (2019). Consecutive bouts of electrical stimulation-induced contractions alter ribosome biogenesis in rat skeletal muscle. *Journal of Applied Physiology*, **126**(6), 1673–1680.
- Kuno, A., Mizuno, S., & Takahashi, S. (2019). KOnezumi: A web application for automating gene disruption strategies to generate knockout mice. *Bioinformatics*, **35**(18), 3479–3481.
- Lapuate-Brun, E., Moreno-Loshuertos, R., Acín-Pérez, R., Latorre-Pellicer, A., Colás, C., Balsa, E., Perales-Clemente, E., Quirós, P. M., Calvo, E., Rodríguez-Hernández, M. A., Navas, P., Cruz, R., Carracedo, Á., López-Otín, C., Pérez-Martos, A., Fernández-Silva, P., Fernández-Vizarra, E., & Enríquez, J. A. (2013). Supercomplex assembly determines electron flux in the mitochondrial electron transport chain. *Science*, **340**, 1567–1570.
- Lund, J., Breum, A. W., Gil, C., Falk, S., Sass, F., Isidor, M. S., Dmytriyeva, O., Ranea-Robles, P., Mathiesen, C. V., Basse, A. L., Johansen, O. S., Fadahunsi, N., Lund, C., Nicolaisen, T. S., Klein, A. B., Ma, T., Emanuelli, B., Kleinert, M., Sørensen, C. M., Gerhart-Hines, Z., & Clemmensen, C. (2023). The anorectic and thermogenic effects of pharmacological lactate in male mice are confounded by treatment osmolarity and co-administered counterions. *Nature Metabolism*, **5**(4), 677–698.
- Magistretti, P. J., & Allaman, I. (2018). Lactate in the brain: From metabolic end-product to signalling molecule. *Nature Reviews Neuroscience*, **19**(4), 235–249.
- Marcinko, K., & Steinberg, G. R. (2014). The role of AMPK in controlling metabolism and mitochondrial biogenesis during exercise. *Experimental Physiology*, **99**(12), 1581–1585.
- Maschari, D., Saxena, G., Law, T. D., Walsh, E., Campbell, M. C., & Consitt, L. A. (2022). Lactate-induced lactylation in skeletal muscle is associated with insulin resistance in humans. *Frontiers in Physiology*, **13**, 1681.
- Mashimo, T., Takizawa, A., Kobayashi, J., Kunihiro, Y., Yoshimi, K., Ishida, S., Tanabe, K., Yanagi, A., Tachibana, A., Hirose, J., Yomoda, J.-I., Morimoto, S., Kuramoto, T., Voigt, B., Watanabe, T., Hiai, H., Tateno, C., Komatsu, K., & Serikawa, T. (2012). Generation and characterization of severe combined immunodeficiency rats. *Cell Reports*, **2**(3), 685–694.
- Matsunaga, Y., Koyama, S., Takahashi, K., Takahashi, Y., Shinya, T., Yoshida, H., & Hatta, H. (2021). Effects of post-exercise glucose ingestion at different solution temperatures on glycogen repletion in mice. *Physiological Reports*, **9**(18), e15041.
- Matsunaga, Y., Tamura, Y., Takahashi, K., Kitaoka, Y. U., Takahashi, Y., Hoshino, D., Kadoguchi, T., & Hatta, H. (2022). Branched-chain amino acid supplementation suppresses the detraining-induced reduction of mitochondrial content in mouse skeletal muscle. *The Federation of American Societies for Experimental Biology Journal*, **36**(12), e22628.
- Memme, J. M., Oliveira, A. N., & Hood, D. A. (2022). p53 regulates skeletal muscle mitophagy and mitochondrial quality control following denervation-induced muscle disuse. *Journal of Biological Chemistry*, **298**(2), 101540.
- Mendoza, B. J., & Trinh, C. T. (2018). Enhanced guide-RNA design and targeting analysis for precise CRISPR genome editing of single and consortia of industrially relevant and non-model organisms ed. Hancock J. *Bioinformatics*, **34**(1), 16–23.
- Muro-Pastor, M. I., & Florencio, F. J. (1992). Purification and properties of NADP-isocitrate dehydrogenase from the unicellular cyanobacterium *Synechocystis* sp. PCC 6803. *European Journal of Biochemistry*, **203**(1–2), 99–105.
- Nakamura, K., Fujii, W., Tsuboi, M., Tanihata, J., Teramoto, N., Takeuchi, S., Naito, K., Yamanouchi, K., & Nishihara, M. (2014). Generation of muscular dystrophy model rats with a CRISPR/Cas system. *Scientific Reports*, **4**(1), 5635.

- Nogami, K., Maruyama, Y., Sakai-Takemura, F., Motohashi, N., Elhussieny, A., Imamura, M., Miyashita, S., Ogawa, M., Noguchi, S., Tamura, Y., Kira, J.-I., Aoki, Y., Takeda, S., & Miyagoe-Suzuki, Y. (2021). Pharmacological activation of SERCA ameliorates dystrophic phenotypes in dystrophin-deficient *mdx* mice. *Human Molecular Genetics*, **30**(11), 1006–1019.
- Ohtsuka, M., Sato, M., Miura, H., Takabayashi, S., Matsuyama, M., Koyano, T., Arifin, N., Nakamura, S., Wada, K., & Gurumurthy, C. B. (2018). i-GONAD: A robust method for in situ germline genome engineering using CRISPR nucleases. *Genome Biology*, **19**(1), 25.
- Park, K. H., Brotto, L., Lehoang, O., Brotto, M., Ma, J., & Zhao, X. (2012). Ex vivo assessment of contractility, fatigability and alternans in isolated skeletal muscles. *Journal of Visualized Experiments*, (69), e4198.
- Philp, A., Macdonald, A. L., & Watt, P. W. (2005). Lactate – a signal coordinating cell and systemic function. *Journal of Experimental Biology*, **208**(24), 4561–4575.
- Rardin, M. J., Wiley, S. E., Naviaux, R. K., Murphy, A. N., & Dixon, J. E. (2009). Monitoring phosphorylation of the pyruvate dehydrogenase complex. *Analytical Biochemistry*, **389**(2), 157–164.
- Robergs, R. A., Ghiasvand, F., & Parker, D. (2004). Biochemistry of exercise-induced metabolic acidosis. *American Journal of Physiology-Regulatory, Integrative and Comparative Physiology*, **287**(3), R502–R516.
- Shi, Q., Karuppagounder, S., Xu, H., Pechman, D., Chen, H., & Gibson, G. (2007). Responses of the mitochondrial alpha-ketoglutarate dehydrogenase complex to thiamine deficiency may contribute to regional selective vulnerability. *Neurochemistry International*, **50**(7–8), 921–931.
- Takahashi, K., Kitaoka, Y.u., & Hatta, H. (2022a). Sex-specific differences in the metabolic enzyme activity and transporter levels in mouse skeletal muscle during postnatal development. *Applied Physiology, Nutrition, and Metabolism*, **48**(5), 361–378.
- Takahashi, K., Kitaoka, Y.u., & Hatta, H. (2022b). Effects of endurance training on metabolic enzyme activity and transporter protein levels in the skeletal muscles of orchietomized mice. *The Journal of Physiological Sciences*, **72**(1), 14.
- Takahashi, K., Kitaoka, Y.u., Yamamoto, K., Matsunaga, Y., & Hatta, H. (2020). Oral lactate administration additively enhances endurance training-induced increase in cytochrome c oxidase activity in mouse soleus muscle. *Nutrients*, **12**(3), 770.
- Takahashi, K., Tamura, Y., Kitaoka, Y.u., Matsunaga, Y., & Hatta, H. (2022). Effects of lactate administration on mitochondrial respiratory function in mouse skeletal muscle. *Frontiers in Physiology*, **13**, 920034.
- Tamura, Y., Kouzaki, K., Kotani, T., & Nakazato, K. (2020). Electrically stimulated contractile activity-induced transcriptomic responses and metabolic remodeling in C2C12 myotubes: Twitch vs. tetanic contractions. *American Journal of Physiology-Cell Physiology*, **319**(6), C1029–C1044.
- Thomas, C., Bishop, D. J., Lambert, K., Mercier, J., & Brooks, G. A. (2012). Effects of acute and chronic exercise on sarcolemmal MCT1 and MCT4 contents in human skeletal muscles: Current status. *American Journal of Physiology-Regulatory, Integrative and Comparative Physiology*, **302**(1), R1–R14.
- Uno, H., Kamiya, S., Akimoto, R., Hosoki, K., Tadano, S., Kouzaki, K., Tamura, Y., Kotani, T., Isemura, M., & Nakazato, K. (2022). Low-frequency electrical stimulation of bilateral hind legs by belt electrodes is effective for preventing denervation-induced atrophies in multiple skeletal muscle groups in rats. *Scientific Reports*, **12**(1), 21275.
- Visser, W. J., Van De Braak, E. E. M., De Mik - Van Egmond, A. M. E., Van Der Burgh, A. C., De Roos, N. M., Jans, I., Van Der Hoef, I., Olieman, J. F., Hoorn, E. J., & Severs, D. (2023). Effects of correcting metabolic acidosis on muscle mass and functionality in chronic kidney disease: A systematic review and meta-analysis. *Journal of Cachexia, Sarcopenia and Muscle*, **14**(6), 2498–2508.
- Wakabayashi, Y., Tamura, Y., Kouzaki, K., Kikuchi, N., Hiranuma, K., Menuki, K., Tajima, T., Yamanaka, Y., Sakai, A., Nakayama, K. I., Kawamoto, T., Kitagawa, K., & Nakazato, K. (2020). Acetaldehyde dehydrogenase 2 deficiency increases mitochondrial reactive oxygen species emission and induces mitochondrial protease Omi/HtrA2 in skeletal muscle. *American Journal of Physiology-Regulatory, Integrative and Comparative Physiology*, **318**(4), R677–R690.
- Wen, Y., Murach, K. A., Vechetti, I. J., Fry, C. S., Vickery, C., Peterson, C. A., Mccarthy, J. J., & Campbell, K. S. (2018). MyoVision: Software for automated high-content analysis of skeletal muscle immunohistochemistry. *Journal of Applied Physiology*, **124**(1), 40–51.
- Wilson, W. A. (2021). Spectrophotometric methods for the study of eukaryotic glycogen metabolism. *Journal of Visualized Experiments*, (174), <https://doi.org/10.3791/63046>
- Wubben, T. J., Pawar, M., Weh, E., Smith, A., Sajjakulnukit, P., Zhang, L.i, Dai, L., Hager, H., Pai, M. P., Lyssiotis, C. A., & Besirli, C. G. (2020). Small molecule activation of metabolic enzyme pyruvate kinase muscle isozyme 2, PKM2, circumvents photoreceptor apoptosis. *Scientific Reports*, **10**(1), 2990.
- Yamada, T., Kimura, I., Ashida, Y., Tamai, K., Fusagawa, H., Tohse, N., Westerblad, H., Andersson, D. C., & Sato, T. (2021). Larger improvements in fatigue resistance and mitochondrial function with high- than with low-intensity contractions during interval training of mouse skeletal muscle. *The Federation of American Societies for Experimental Biology Journal*, **35**(11), e21988.
- Yang, Z., Yan, C., Ma, J., Peng, P., Ren, X., Cai, S., Shen, X., Wu, Y., Zhang, S., Wang, X., Qiu, S., Zhou, J., Fan, J., Huang, H.e, & Gao, Q. (2023). Lactylome analysis suggests lactylation-dependent mechanisms of metabolic adaptation in hepatocellular carcinoma. *Nature Metabolism*, **5**(1), 61–79.

- Zhang, D.i, Tang, Z., Huang, H.e, Zhou, G., Cui, C., Weng, Y., Liu, W., Kim, S., Lee, S., Perez-Neut, M., Ding, J., Czyn, D., Hu, R., Ye, Z., He, M., Zheng, Y. G., Shuman, H. A., Dai, L., Ren, B., Roeder, R. G., Becker, L., & Zhao, Y. (2019). Metabolic regulation of gene expression by histone lactylation. *Nature*, *574*(7779), 575–580.
- Zhu, A., Romero, R., & Petty, H. R. (2010). A sensitive fluorimetric assay for pyruvate. *Analytical Biochemistry*, *396*(1), 146–151.

## Additional information

### Data availability statement

Any additional information required to reanalyse the data reported in this paper is available from the lead contact upon reasonable request.

### Competing interests

The authors declare they have no competing interests.

### Author contributions

Y.T.: conception or design of the work, acquisition, analysis or interpretation of data for the work, drafting the work or revising it critically for important intellectual content. E.J., K.K. and K.N.: acquisition, analysis or interpretation of data for the work, drafting the work or revising it critically for important intellectual content. T.K.: acquisition, analysis or interpretation

of data for the work, drafting the work or revising it critically for important intellectual content. All authors have read and approved the final version of this manuscript and agree to be accountable for all aspects of the work in ensuring that questions related to the accuracy or integrity of any part of the work are appropriately investigated and resolved. All persons designated as authors qualify for authorship, and all those who qualify for authorship are listed.

### Funding

This work was supported by a Nippon Sport Science University Research Grant (to Y.T.) and a Japan Society for the Promotion of Science (JSPS) Grant-in-Aid for Scientific Research (to Y.T., no. 21H03332).

### Keywords

exercise, glycolysis, high-intensity interval training, lactate, metabolism, mitochondria, monocarboxylate transporter, skeletal muscle

## Supporting information

Additional supporting information can be found online in the Supporting Information section at the end of the HTML view of the article. Supporting information files available:

### Peer Review History

### Supplemental information